Design of ankle-knee prostheses using predictive simulations

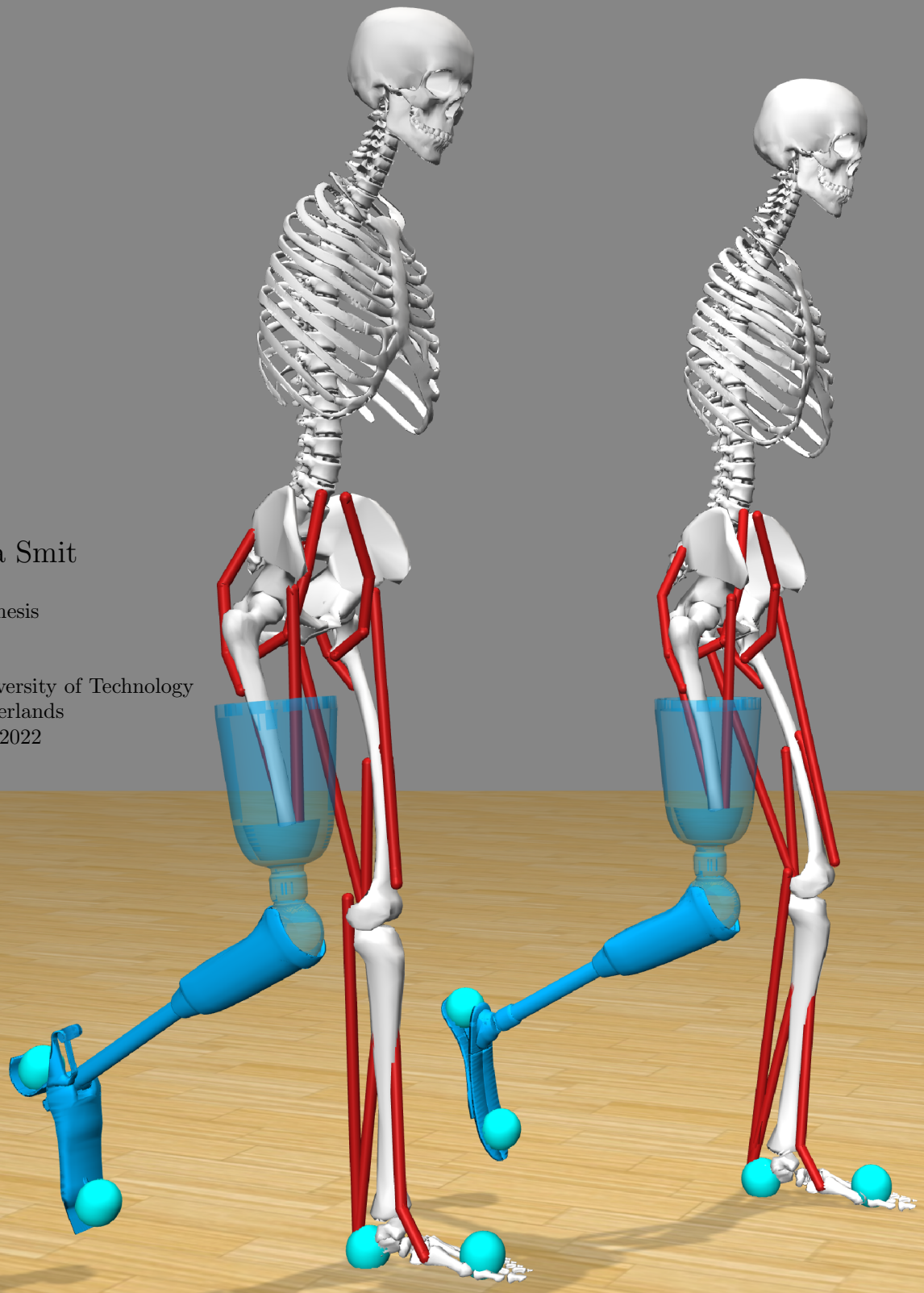

Nerissa Smit

Master Thesis

Delft University of Technology
The Netherlands
February 2022

Design of ankle-knee prostheses using predictive simulations

by

Nerissa Smit

to obtain the degree of Master of Science
in Biomedical Engineering
at the Delft University of Technology,
to be defended publicly on Tuesday February 22, 2022 at 02:00 PM.

Student number:	5169585
Project duration:	January, 2021 – February, 2022
Supervisor:	Dr. ir. A. Seth
Thesis committee:	Dr. ir. G. Smit
	Dr. T. Geijtenbeek
	Dr. ir. R. Happee

TU Delft Delft University of Technology

Contents

Abstract

Background. There is an increasing need for transfemoral prostheses that provide gait support, stability, safety and comfort. Although there are many prostheses available in different levels of complexity and price, there is still room for improvement. It has been proved that the cost of transport (CoT) for walking is significantly increased for transfemoral amputees with respect to their healthy peers. Assisting push-off is one of the main challenges in prosthesis design. Push-off is normally achieved by plantarflexion of the ankle joint. Prosthesis designs should aim to restore this function in order to lower the amount of energy needed for walking.
Objective. This study aims to investigate the effect of prosthesis design on the gait pattern through musculoskeletal modelling and predictive simulations. Two prosthesis designs are modelled for these purposes, after which several variations on these models are made. It is hypothesised that the prosthesis that assists in push-off through ankle plantarflexion, should result in a gait pattern that is closer to a healthy one. It should also decrease the CoT. Furthermore, we aim to evaluate the use of modelling and simulations in the customisation of prostheses.
Method. OpenSim was used to create a total of eight models based on a model with 9 degrees of freedom and 18 muscles: a healthy person, a conventional prosthesis model, two scaled versions of the conventional prosthesis model, the walkMECH prosthesis and three variations on the walkMECH. SCONE was used to find an optimal gait pattern for each of the models through the CMA-ES method. CoT-, gait-, degrees of freedom- and reaction force objectives were minimised. The results were evaluated by comparing the CoT, joint angles, ground reaction forces and muscle activation of each model.
Discussion. The CoT for the healthy model was found to be higher than reported before, based on both experimental and simulation studies. As a result, we have little confidence in the CoT estimation of our models. This is further exacerbated by the finding of a lower CoT for the conventional prosthesis than for the healthy model, in contrast to earlier reports. The results for most other measures were irregular, making it difficult to draw conclusions from them. It is expected that the predictive optimisations did not reach a global minimum, and that the results are therefore not accurate. Future research should aim to solve this problem. It should also be attempted to find the cause of the difference in CoT between our simulations and those of others.
Conclusion. No conclusions could be drawn from the results. Nonetheless, there is a clear potential for the use of musculoskeletal modelling and predictive simulation in the investigation of the effects of prosthesis design on gait.

1 Introduction

1.1 Transfemoral amputation

In the European Union, approximately 17-26 in 100.000 persons per year undergo lower limb amputation proximal to the toes [1]. Unfortunately, these numbers will be rising in the upcoming years [2,3]. The main cause for amputation is diabetes mellitus, involving poor wound healing and vascular problems. A minority of patients undergo amputation due to trauma and malignancy. On top of that, shortened limbs can also be the result of congenital limb defects [2,4,5]. Considering the large and still rising amount of people with a lower limb amputation, prosthetic devices that fulfil the functions of a missing limb are much needed.

It has been shown that walking with a prosthesis requires more effort than walking with two intact legs [6–8]. This can easily be seen in the unconventional gait pattern, but can also be quantified using the energy cost of transport (CoT) and the self-reported effort by patients. The level of amputation, aetiology and the type of prosthesis used all greatly influence the needed effort for walking and the preferred walking speed [6,7]. In general, patients with a transfemoral amputation or knee disarticulation have a harder time walking than patients with a below-knee amputation. This is because not only the ankle joint, but also the knee joint needs to be replaced by a mechanical substitute. Without actuation, these joints can not provide as much energy input and stability as the anatomical joints, which are actively controlled by muscles. In this paper, stability will be defined as resistance to falling, mostly through resistance of knee flexion.

1.2 Lower limb prostheses

Depending on the height of the lower limb amputation, between one and three prostheses are needed. We focus on transfemoral amputees, and will therefore discuss foot- and knee prostheses. For both prostheses, there are multiple categories available, based on the level of complexity. The simplest prostheses, such as the conventional foot and locked knee, provide the least amount of push-off support, but are generally quite stable. These are usually the least expensive prostheses [9,10]. On the other hand are bionic feet and microprocessor controlled knees [7,11]. These advanced prostheses make use of active actuation and sensor information. Because these prostheses are several times more expensive and therefore not often used, they will not be discussed any further in this paper.

Energy storage and return (ESAR) feet are most commonly used. The energy storage and return properties of an elastic material assist a push-off motion of the ankle. The stiffness of the foot can be customised based on the activity level and weight of the patient [12]. However, ESAR feet can be less stable than conventional prosthetic feet and they do not provide the same level of support an anatomical foot does.

While the locked knee prosthesis provides a high level of stability, it does not permit a normal gait pattern in any way. Conventional mechanical knees can have either monocentric or polycentric joints. Passive elements, such as a hydraulic or pneumatic system can be implemented for more support and stability. However, these mechanical, passive prostheses still do not completely provide the push-off power and stability needed. Furthermore, the effect of passive elements relative to each other is mostly unknown. No research is found regarding the effect of the exact application, or the location of the attachments and mechanical properties, of a component.

None of the previously mentioned prostheses are able to mimic the function of an anatomical leg to its full potential. One of the main reasons might be that there is no interaction between the joints. The few combined ankle-knee prostheses that have been designed so far seem to be promising, but very little quantitative data are available [13–16].

1.3 Prosthesis design

Despite the large number of papers dedicated to design and evaluation of prostheses, there is no clear overview on the effect of prosthetic design on the gait pattern, cost of transport and joint loads. This

makes it difficult to decide which designs should be used for the realisation of an optimal prosthesis and which components can be modified in order to fit a patient best.

An extensive design process is needed for the development of previously mentioned and future prosthetic devices [17]. Creating a good prosthesis design requires a large amount of time and labour. In order to evaluate the design, physical representations of the design might need to be fabricated. Furthermore, the design needs to be tested by amputee patients or healthy participants with a converter.

To decrease the time needed for physical changes to the prosthesis throughout iterations and experiments, it would be beneficial to use an alternative design and test method. Musculoskeletal models and predictive simulations could potentially offer a solution. A prosthetic prototype design can be created, optimised and tested digitally. The open source software OpenSim [18, 19] and SCONE [20] can be used for these purposes.

1.4 Previous studies using OpenSim and SCONE

OpenSim and SCONE have been validated for both healthy person and prosthesis simulations. Ong et al. [21, 22] have proved that musculoskeletal modelling and predictive simulations of a healthy individual create realistic results. They found kinematic and kinetic trends that matched experimental data. Furthermore, the CoT of their model matched experimental data for several walking speeds.

OpenSim was used before to create a transtibial amputee model [23]. After creating the model, LaPré et al. used inverse kinematics and inverse dynamics to apply experimental data to the model and be able to evaluate the gait pattern. Residuum-socket kinematics were also reconstructed through this method. The simulations resulted in kinematics similar to those found in experimental data. A 4 degrees of freedom (DOF) interaction between the stump and the socket generally resulted in realistic movements. However, residuum-socket interactions normally greatly depend on the type of socket suspension [23]. Because of this dependency and the fact that this 4-DOF interaction might cause longer simulation times in SCONE, it was decided to use a rigid joint in this paper.

1.5 Prosthesis design using predictive simulations

This study aims to investigate two research goals. The first and main goal is to explore the effect of prosthetic design on amputee gait. The effect will be measured in terms of CoT, kinematics, kinetics and muscle activation. It is expected that the simulation results show a higher CoT for the models walking with a prosthesis, along with deviations in the kinematics and kinetics. Furthermore, it is expected that a clear improvement in the gait pattern and CoT will be present when supporting elements are added to a prosthesis [24–26]. In order to investigate this statement, two different prosthesis designs will be modelled. The first prosthesis is a 'conventional' prosthesis, which does not assist in the push-off phase. Likewise, no components are added that prevent knee flexion during stance. The simulation results of this prosthesis will serve as a baseline to compare the second prosthesis to. The second prosthesis design modelled in this study is the walkMECH, designed by Unal et al. [14]. In this prosthesis, two springs are added as supporting element for push-off. This prosthesis was chosen because it is a combined ankle-knee prosthesis, belonging to the small group of designs that have shown promising results of combined joints. We limited this paper to passive prosthesis to limit the complexity of the model. All other combined ankle-knee prostheses found were powered, and were therefore not suitable for this paper.

The secondary goal of this study is to investigate the customisation of prostheses. Because every patient has different anthropometry, amputation height and compensation mechanisms, a prosthesis might perform differently for each individual. Two scaled models with a conventional prosthesis will be created and evaluated. The scaled models are based on the anthropometry of an average male and female body [27]. It is expected that all parameters will be similar for each model, but still present slight differences. Furthermore, design parameters of the walkMECH will be changed to attempt to model customised prostheses. The biarticular spring, which can normally slide forwards and backward on the distal side, will be fixated at the two ends of the slider. A third variation will

be created by changing the tension springs into compression springs. It is expected to find larger parameter deviations for these variations. If the adapted support components provide larger push-off power and stance support, the CoT is expected to decrease. Furthermore, the kinematics and kinetics are expected to be closer to the values of a healthy person. These expectations are based on the same reasoning as used in the first research question.

Based on the results of the simulations, the possible application of predictive simulations in the design and customisation of prostheses will be discussed.

2 Materials and methods

To investigate the effect of adding push-off assisting elements to a prosthesis, predictive simulations were run for the conventional and walkMECH designs. A healthy person model was also created and simulated in order to evaluate whether the effects of the prosthesis designs are positive or negative. The simulation results of the prosthesis models should be closer to that of the healthy model if the prosthesis better assists push-off.

An improved gait pattern, if present, will be visible as the joint angles of both the intact and prosthetic leg being closer to healthy angles. The lack of push-off by the prosthetic knee and ankle needs to be compensated for by the hip muscles of the same leg and all of the contralateral leg. The prosthetic joint angles will most likely be different from the healthy joint angles. For the conventional prosthesis, all joint movements will result from the forward swing of the leg, facilitated by the hip and the muscles around it. Therefore, it can be expected that the muscle actuation of these muscles is higher for the prosthetic leg than for a healthy leg. If the springs in the walkMECH indeed add push-off power, the hip muscles of the prosthetic leg should be activated less.

2.1 Software

OpenSim is open source simulation software that can be used to model and simulate multibody systems. It is very suitable for simulating (a part of) the human body, because it includes components that can mimic the function and dynamics of human tissues, such as muscles and tendons. Furthermore, it facilitates the simulation of several mechanical components, such as springs [18]. Models made in OpenSim can then be loaded into SCONE for predictive simulations. SCONE is a "Simulated Controller Optimization Environment". Based on controls and weighted cost functions, the program optimises the movement of a model using the Covariance matrix adaptation evolution strategy (CMA-ES) [20, 28].

2.2 Transfemoral amputee model

We considered two healthy person models on which to base the transfemoral amputee model. The first model was already validated, but did not give accurate results in preliminary simulations [22]. The second model was previously used for transtibial amputee simulations, and was therefore expected to be useful for out transfemoral amputee model as well [23]. The transfemoral amputee model was created by altering a healthy person model with 9 DOF and 18 muscles [18, 19]. In order to make a unilateral transfemoral amputee, all following changes were made to the right side of the model only.

The femur was shortened to approximately two thirds of the original length. Accordingly, the mass of the femur was reduced to approximately 64% of the normal mass. The mass reduction was based on experimental data [29] and the calculations in the appendix (A.1). Furthermore, the centre of mass (CoM) of the femur was moved slightly more proximal. All bones below the knee were removed from the model.

Furthermore, all muscles that actuate the ankle were removed. The rectus femoris and hamstrings muscles, which normally control the hip and knee, were reinserted to the transected end of the femur. It was attempted to retain the original function of these muscles with regard to the hip. This was done by trying to maintain the angle of the muscle over the joint. However, this is likely unrealistic,

since the amputation procedure is not standardised. Not only is the amputation procedure dependent on the surgeon, but also on the patient. For instance, when a limb needs to be amputated due to trauma, tissues are often severely damaged. This means that the surgeon needs to work with what is left, as opposed to starting off with an intact leg. Furthermore, the distance between the muscle and the joint is most likely different because the insertion point is more proximal after amputation. This results in a slightly smaller moment arm.

The properties of the upper-leg muscles that were shortened were also adjusted. The tendon slack length and maximum isometric force that can be exerted by the shortened muscles was decreased, based on the reduction of muscle length. The rectus femoris muscle was shortened from 0.4063 to 0.3110 m. Therefore, the scaling factor for this muscle was $\frac{0.3110}{0.4063} = 0.7654$. The hamstrings were shortened from 0.4046 to 0.2468 m, resulting in a scaling factor of $\frac{0.4046}{0.2468} = 0.6101$. Both the maximum force and the tendon slack length of the intact muscles were multiplied by their respective scaling factor to find the values for the amputated muscles. The optimal fibre length was not changed. If the tension of the amputated muscle is made identical to that of the intact muscle, the optimal fibre length should not change significantly [30].

The muscles that cross the knee only, the vasti and biceps femoris short head, were removed. The lower half of the model with all new muscle insertions can be seen in Fig. 1.

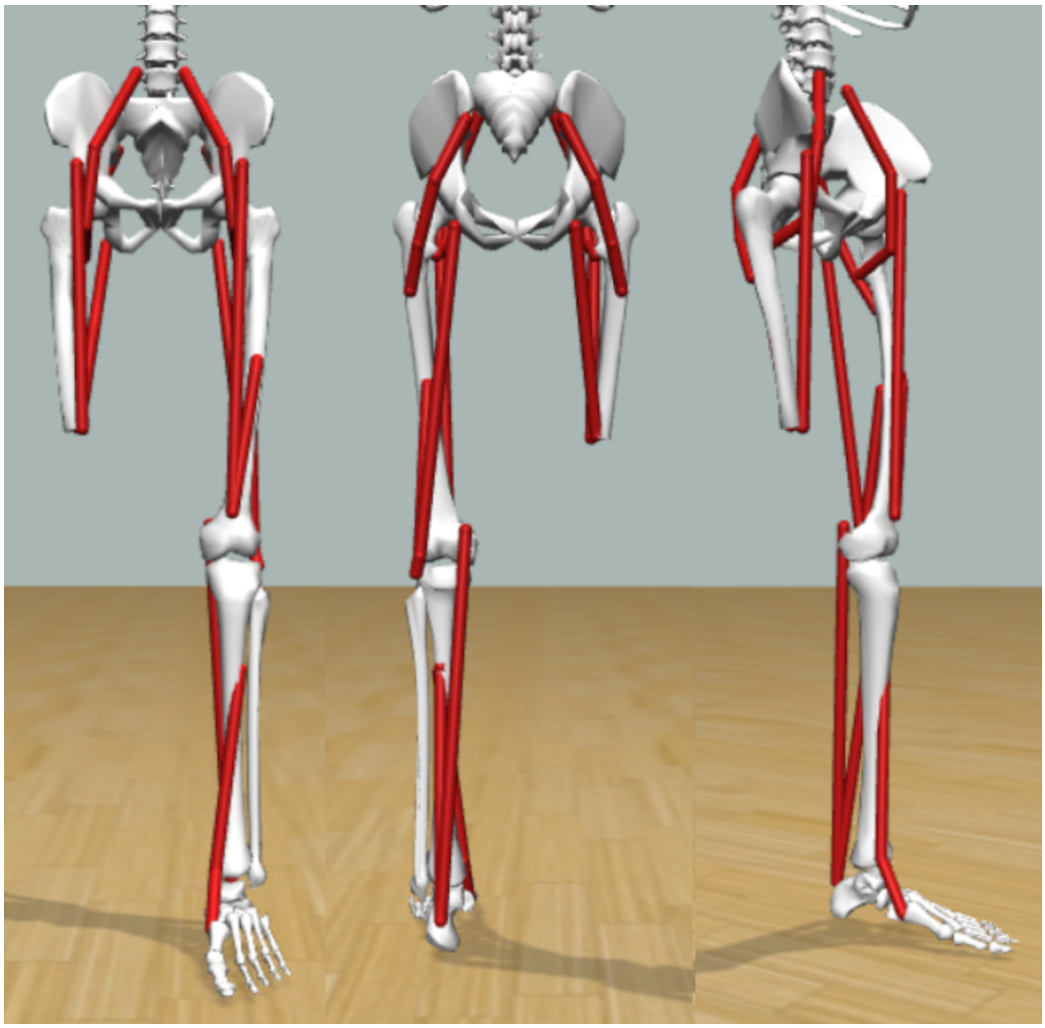

Fig 1. Transfemoral amputee model. Front, back and diagonal view of the OpenSim model of a right side transfemoral amputee. Based on a 9 DOF, 18 muscle model [22].

2.3 Prosthesis socket

A generic socket was visualised using the socket of an existing transtibial amputee model [23]. The socket was scaled to fit for an upper leg. The femur and socket interaction was modelled as a weld joint to limit the complexity of the model. The mass of a generic socket is difficult to find in literature. Therefore, the mass was set so that the mass of the amputated femur (5.96 kg) and socket (3.34 kg) together were equal to that of the intact upper leg (9.30 kg). Although this is most likely an overestimation of the actual mass, it might be better to overestimate the mass than to underestimate it. This is hypothesised based on the fact that more mass generally means that more energy is needed to move it. The calculations used to find the inertia of the socket and all other introduced geometries can be found in the appendix (A.2).

2.4 Conventional prosthesis

The conventional prosthesis that was modelled was one with a single axis knee and single axis ankle (see Fig. 2a). No mechanical aids were added, apart from torsional springs modelled as limit forces to ensure the range of motion of the knee and ankle was not exceeded. In the results, the model will be referred to as CM.

The knee joint was represented by a pin-joint with a range between 100° of flexion and 9° of (over)extension. These angular limits were enforced by limit forces. The initial values of the limit force was set to an upper stiffness of 100N/deg at 1° extension and a lower stiffness of 60N/deg at 100° flexion. The damping was set to 0.2Nm/deg/s and the transition to 1 degree. However, the stiffness and damping were allowed to be optimised, as is described in section 2.8.

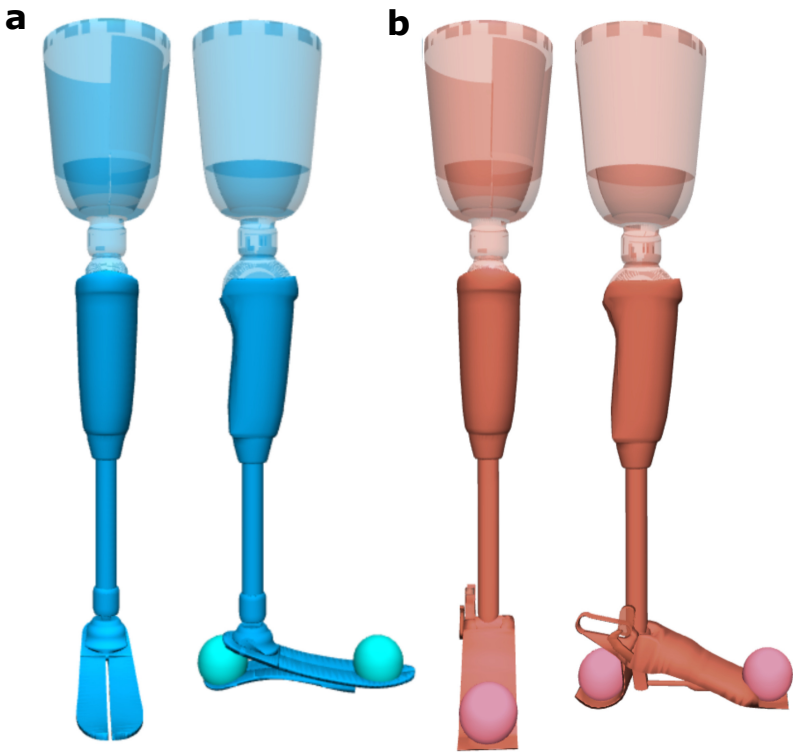

Fig 2. Conventional prosthesis and walkMECH design. a) Visual representation of the conventional prosthesis (front and side view) and b) the walkMECH (front and side view). It should be noted that the springs are not visualised. The colours of the prostheses are conform the colours of their results in all figures.

The lower leg was shaped like a generic prosthesis. The mass of the prosthetic lower leg was based on that of the lower leg by Unal et al. [14]. The CoM was determined by visual estimation. The ankle joint was modelled by means of a pin-joint with an angular range between 60° of dorsal- and plantarflexion. This range is equal to that of the contralateral, intact ankle. The angular limits were enforced by limit forces, of which the initial upper stiffness was set to 50 N/deg at 10° of dorsalflexion. The initial lower stiffness was set to 75 N/deg at 20° of plantarflexion. The initial damping was set to 0.2 Nm/deg/s and the transition to 1 degree. The limit angles were based on the minimum and maximum angles in the experimental results from Winter [26].

For the foot prosthesis, the model from the existing transtibial amputee model [23] was used with some minor geometrical alternations. The energy storage and return properties of this foot were mimicked by the stiffness and damping of the contact spheres at the heel and toe of the foot geometry [23]. The contact spheres were set to interact with the ground by means of Hunt Crossley forces [31]. This is the same as for the intact leg. The mass, CoM and inertia of all conventional prosthetic components can be found in Table 1. The mass of the foot was again made equal to that of the foot of the prosthesis by Unal et al. [14].

Table 1. Properties of the prosthetic components for a conventional prosthesis. The xy, xz and yz components of the inertia were all made zero and therefore left out of the table.

	Socket	Lower leg	Foot
Mass (kg)	3.34	1.44	1.75
CoM	[0 -0.03 0]	[-0.006 -0.140 -0.005]	[0.015 0.035 0]
Inertia	[0.0407 0.0144 0.0407]	[0.0190 0.0002 0.0190]	[0.0004 0.0019 0.0020]

2.5 WalkMECH

The walkMECH is a combined ankle-knee prosthesis based on two single-axis joints and two compression springs (Fig. 2b) [14]. The first spring is biarticular and is used to absorb energy during the swing phase and transfer this energy to the ankle. It also absorbs some energy during midstance. All stored energy is released in the push-off phase. This spring attaches to the upper leg and a slider on the foot and runs along the lateral side of the prosthetic leg. Because of the slider, the spring can change its path as a direct result of the position of the segments. The mechanical blocking mechanism is implemented to catch and release the slider at the correct moments (Fig. 3). A slight indentation at the posterior side of the slot keeps the slider at the back longer. The sliders enable a change in moment arm of the spring to both the ankle- and knee joint, which also changes the function of the springs.

The second spring is responsible for absorbing energy during early- and mid-stance and releasing this energy during push-off. The spring runs between a distal extension of the lower leg, at about 3 cm from the ankle joint, to the front of the foot. Therefore, it only controls the ankle motion. In the results, the model will be referred to as WM.

In the upper part of the side plates of the foot, a long slot was made for a slider to slide through. A small slider was made to attach the biarticular spring to. This slider was initially attached to the foot with a slider joint that enabled a movement along the x-axis only. Therefore, the frame of the slider was rotated 7.5° about its z-axis. The range of the sliding motion was not specified in the article by Unal et al. [14] because it was manually customised for the amputee using the prosthesis. The range was estimated to be approximately 4.6 cm. The indentation at the back of the slot was created as a curved slider path, which can be found in Fig. 4.

The blocking system was modelled as a magnetic force at the front of the sliding slot. This was done because the mechanical system is too complex to model accurately. In particular, the contact between the components is difficult to achieve. The magnetic force was modelled to function as the mechanical blocking mechanism (Appendix A.3).

The biarticular spring consisted of two linear springs inside of one another with different slack lengths and stiffness, to achieve a bi-linear force-length relationship (see Fig. 5). The springs only

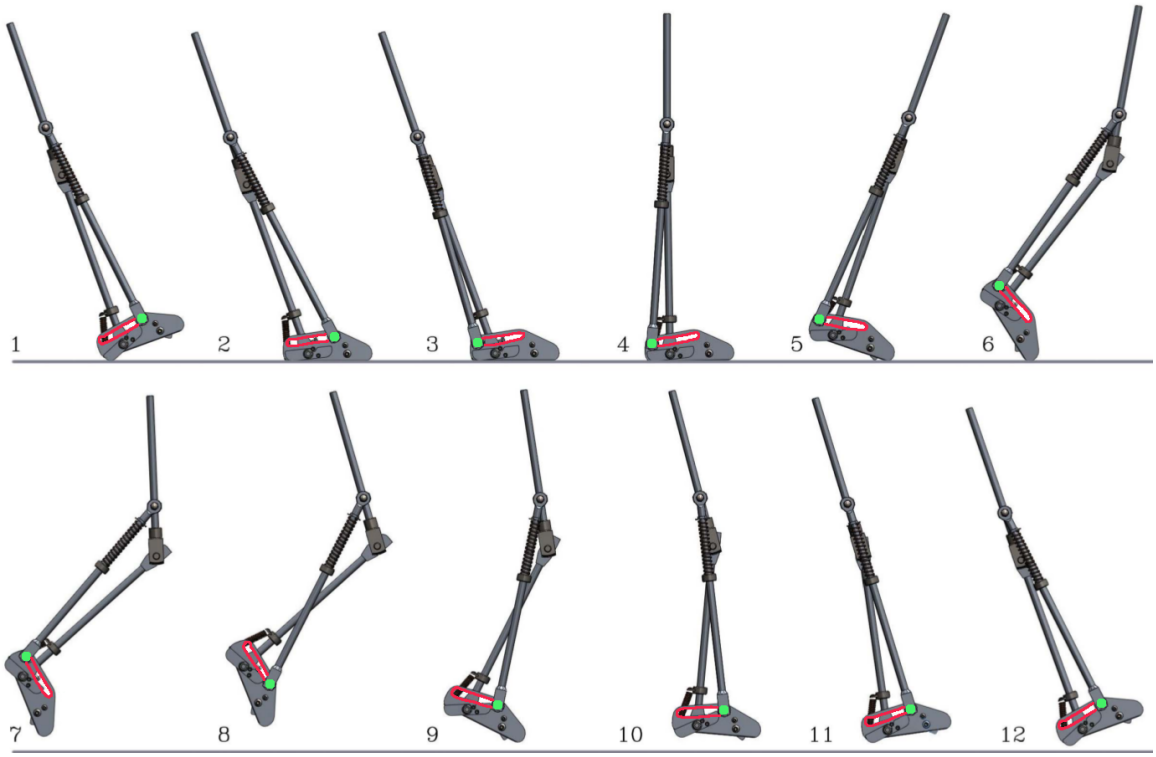

Fig 3. WalkMECH gait pattern. Schematic representation of the gait pattern of the walkMECH prosthesis as reported in the paper by Unal et al. [14]. The green dot marks the location of the slider, the red lines mark the slider slot.

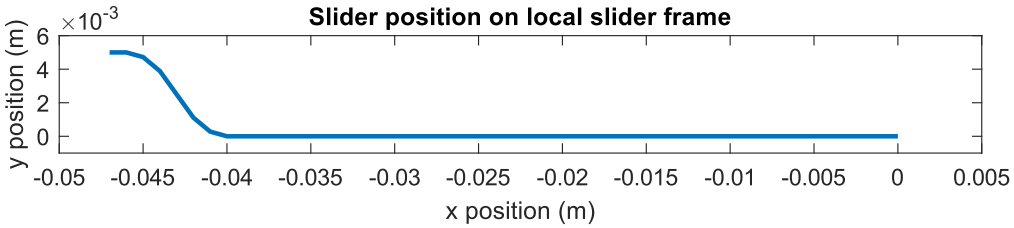

Fig 4. Slider path. Slot of the slider with a upwards curve at the back. The path was created with a custom joint with step function for the translation in y direction.

take up a small portion of the distance between the attachment points. The biarticular spring was attached to the posterior side of the socket and the middle of the slider. The stiffness of the outer and inner spring were 12.000 and 183.000 N/m respectively. The rest lengths of the springs were set to 0.1 and 0.075 m respectively.

For the spring that crosses the ankle only, the stiffness was set to 133.000N/m. The rest length of the spring was reported to be the length of the spring at the start of roll over of the prosthetic leg and was set to 0.046 m. The exact settings of the springs can be found in the appendix (A.3).

The mass of the prosthetic components were based on the mass reported in the paper and patent [14, 32]. The mass of the lower leg was reported to be 1.44 kg and that of the foot to be 1.05 kg. The mass of the springs and sliders was not reported. Therefore, the mass of the foot was distributed over the foot and sliders and can be found in Table 2. In order to be able to accurately simulate the movement of the sliders, mass is needed. The mass of the slider was increased slightly to make the movement more realistic, and therefore the mass of the foot itself was equally decreased. The CoM of all components was estimated by visual inspection of the model.

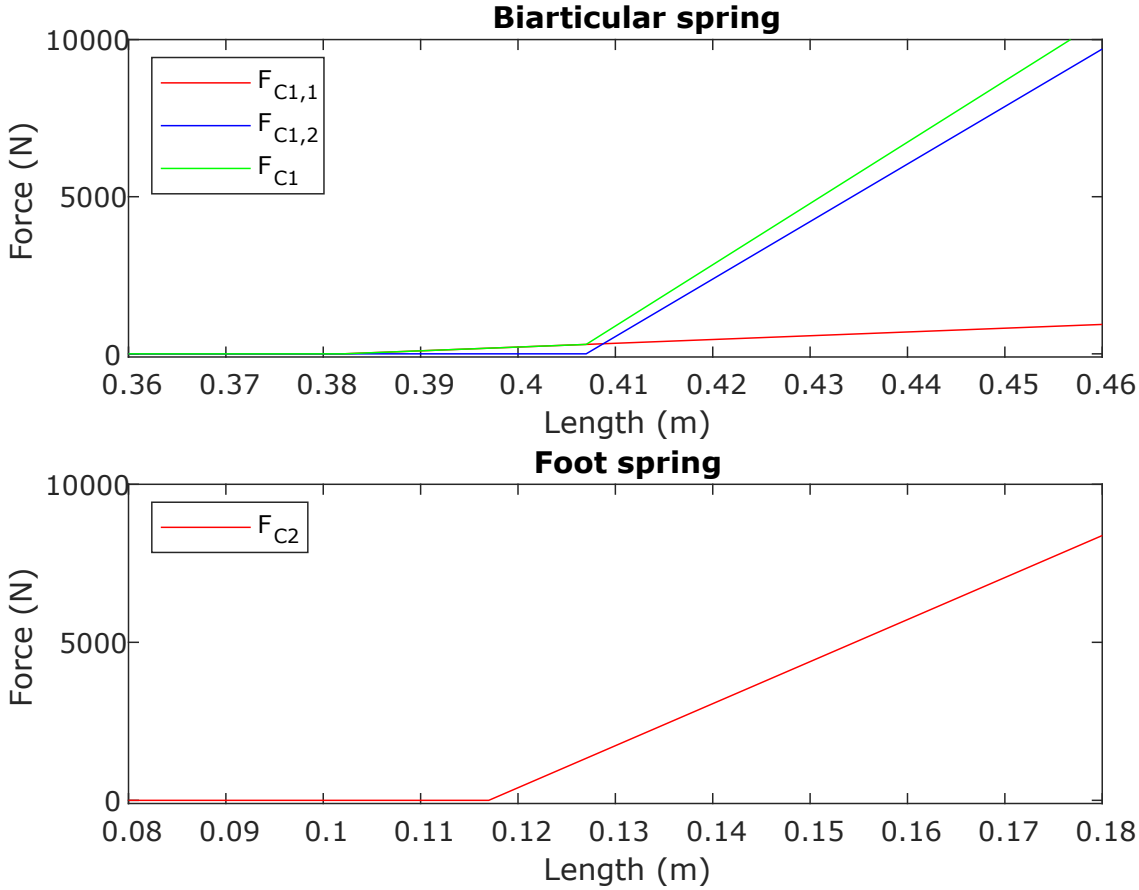

Fig 5. Spring forces. Force-length relationship of the biarticular and foot springs. The lenght is the total distance between the attachment points of the spring. Two linear springs were used to create the bilinear biarticular spring.

Table 2. WalkMECH properties Properties of the prosthetic components for the walkMECH prosthesis by Unal et al. [14]. The xy, xz and yz components of the inertia were all made zero and therefore left out of the table.

	Socket	Lower leg	Foot	Slider
Mass (kg)	3.34	1.44	0.53	0.52
CoM	[0 -0.03 0]	[-0.006 -0.14 -0.005]	[0.05 -0.075 0.005]	[0 0 0]
Inertia	[0.0407 0.0144 0.0407]	[0.0132 0.0001 0.0132]	[0.0010 0.0034 0.0031]	[0.0000 0.0000 0.000]

2.6 Customisation of the conventional prosthesis

In order to test the effectiveness of the prosthesis for different patients, the conventional prosthesis model was scaled. Two scaled models were made: one male subject with a height of 182 cm and a mass of 85 kg and one female subject with a height of 165 cm and a mass of 75 kg. In the results, the models will be referred to as CMm and CMf respectively.

The scaling tool in OpenSim was used to scale the model. This tool requires scaling factors, which are dependent on the initial length and desired length of the body segments. The initial length of each segment was determined by placing a marker at each end of the segment and calculating the difference in coordinates. The desired lengths of the segments were determined according to the mean segment lengths with respect to total body height in order to achieve the correct segment proportions [27].

2.7 WalkMECH variations

In order to evaluate the effect of design on the functioning of the prosthesis, multiple configurations were modelled. The best working version of the original prosthesis was used to create the configurations. From there on, the properties of the spring were changed, as well as the placement of the spring attachments.

The first variation made was one in which the slider was locked to the front of the slot. In order to do so, the slider joint was substituted by a weld joint. The second variation was made in the same way, but with the slider locked at the back of the slot. These variations will be referred to as WMf and WMb respectively.

A third variation was made by taking the exact same model and optimisation scripts, but reversing the functionality of the compression springs. Instead of delivering force upon lengthening, the biarticular springs now delivered force upon shortening. This should provide stability throughout the stance phase. All parameters of the spring, including the spring constants and the slack lengths, remained unchanged. The reverse spring model will be referred to as WMr.

2.8 Predictive simulations

All predictive simulations were conducted using SCONE. Several files are needed for one simulation. An overview of the file contents can be found in the appendix (A.4). The original files were provided by Geijtenbeek [20] and adapted for models with a transfemoral amputation and prosthesis.

The predictive simulations aimed to solve an optimisation problem with the following objective functions in order of highest to lowest priority:

- The gait pattern should be as close to a normal gait pattern as possible
- The ground reaction forces should be as low as possible
- The gait pattern should cost a minimum amount of energy
- The joint angles should not exceed healthy boundaries

The control parameters were optimised to minimise this objective function, which should result in a gait pattern within a specific range of velocities without falling. The minimum walking velocity was chosen to be 0.8 m/s, comparable to experimental results [7]. No maximum walking velocity was defined, to allow the objective to find the optimal velocity of the model. The energy cost, including the cost of transport, was minimised through the effort measure, using the Uchida2016 method [33]. The joint angles were kept within range by optimising the DOF measure. The ground reaction force(GRF) was minimised by optimising the reaction force measure [34].

In order to solve the optimisation problem, a control strategy was defined. The controller allows parameters to be changed within a set range so that the objective functions can be minimised and an optimal solution can be found. The controller include reflexes and control parameters for all muscles in the model.

In early stages of the musculoskeletal model design process, simulation results were used to identify problems in the model. When the final version of the model was reached, the method below was used.

To attempt to find the global minimum, ten simulations were run with the initial settings, without initial parameter input. The best result was then chosen and used as seeds for another set of ten simulations. The best result of these simulations were then imported in Matlab for evaluation.

2.9 Design comparison

Predictive simulation results of all models were compared to those of a healthy person. The results of a healthy model were already verified [22]. We therefore assume that results of prosthesis model simulations being similar to those of the healthy model is positive. In the results, the healthy model

will be referred to as HM. Experimental joint angles were copied from Mentiplay et al. [35] and included in the results to represent realistic deviations from the simulation results of HM. These experimental data were chosen because they are walking speed specific and recent [35]. Since the minimum walking speed of the models was set to 0.8 m/s, the reference angles were chosen to be those measured at a walking speed between 0.8 and 1.0 m/s.

All simulations were compared for walking velocity, step frequency (and stride length) and cost of transport of all models were compared to each other. Furthermore, the joint angles, ground reaction forces and muscle activation patterns were compared. This was done for both the intact and prosthetic leg.

In order to easily compare the data, a MATLAB script was made to load and process SCONE's output. After loading the data, one gait cycle was selected from the middle of the simulation, where each cycle is approximately the same. In accordance with the reference data, the cycle was taken from heel strike to heel strike of the same foot. The timing of heel strike was found by searching for the sample where the GRF became non-zero. To be able to compare both the intact and the prosthetic leg more easily, a separate cycle was be selected for each foot. Furthermore, each cycle time was normalised to represent 0-100% of the gait cycle.

3 Results

The results for each model will be discussed per outcome measure. The measures discussed are the CoT, the joint angles (kinematics), GRF and muscle activation. Other measures can be found in Table 3. It should be noted that for HM, the optimal gait pattern was found at a considerably higher walking speed than for all other models.

Table 3. Simulation results. Simulation results for all optimisations. The walking speed, step frequency and stride length were calculated using the distance, total time and step count.

	HM	CM	CMm	CMf	WM	WMb	WMf	WMr	
Walking speed	0.987	0.907	0.914	0.915	0.828	0.949	0.883	0.907	m/s
Step frequency	1.550	1.400	1.400	1.400	1.550	1.750	1.700	1.550	Hz
Stride length	0.640	0.648	0.653	0.653	0.534	0.558	0.519	0.585	m
Cost of transport	4.913	4.165	4.000	4.092	5.310	4.483	6.431	4.532	J/kg/m

3.1 Cost of transport

3.1.1 Healthy model

The CoT for HM proved to be 4.81 J/kg/m. This is significantly higher than the value reported by Ong et al. [22] for the same walking speed, which was approximately 3.00 J/kg/m. In that article, the model and optimisation method were validated by comparing the simulation results with experimental data. It would therefore be expected that the value resulting from the model and simulations in this study would be closer to the values of Ong et al. [22]. Because of this large difference, we have little confidence in these results for the CoT.

3.1.2 Conventional prosthesis model

The CoT for CM was 4.18 J/kg/m, which is significantly lower than the Cot for HM. This is not in line with the expectations based on experimental data [7]. While there are fewer muscles in the amputee model that can be active and therefore use energy, the energy expenditure should be larger than for the healthy model. Again, we have little confidence in these results.

For the male and female models, CMm and CMf, the CoT were lower at 4.00 and 4.10 J/kg/m respectively. This is likely due to them having a larger mass and different mass distributions.

3.1.3 WalkMECH prosthesis model

The CoT for WM was much higher than for the healthy and conventional models. Moreover, the WM performed worse than two of the variations based on the model. The CoT of the WM was 5.31 J/kg/m, that of WMf was 4.48 J/kg/m and that of WMr was 4.52 J/kg/m. Only WMb performed worse than WM, with a CoT of 6.43 J/kg/m. This suggests that the design chosen for the walkMECH was not the optimal design, or that the design was not modelled correctly. Furthermore, the WM was designed to support the amputee in their gait pattern and should decrease the CoT with respect to walking with a non-supporting prosthesis, such as the CM. However, the CoT of WM was much higher than that of CM, suggesting that this goal was not reached. We have little confidence in these results.

3.2 Joint angles

3.2.1 Healthy model

The joint angles for HM can be found in Fig. 6. As expected, the joint angles were completely symmetric for HM. The hip angles were completely within range of the experimental data. Although the knee and ankle angles were mostly within range as well, there were a few deviations.

3.2.2 Conventional prosthesis model

All joint angles for CM can be found in Fig. 6 and 7. The hip angles of the intact leg of CM were smaller in both directions than those of HM (visible as lower amplitude). In contrast, the hip angles of the prosthetic leg were larger than those of HM. The hip angles of CMm and CMf for both the intact and prosthetic leg were similar to those of CM.

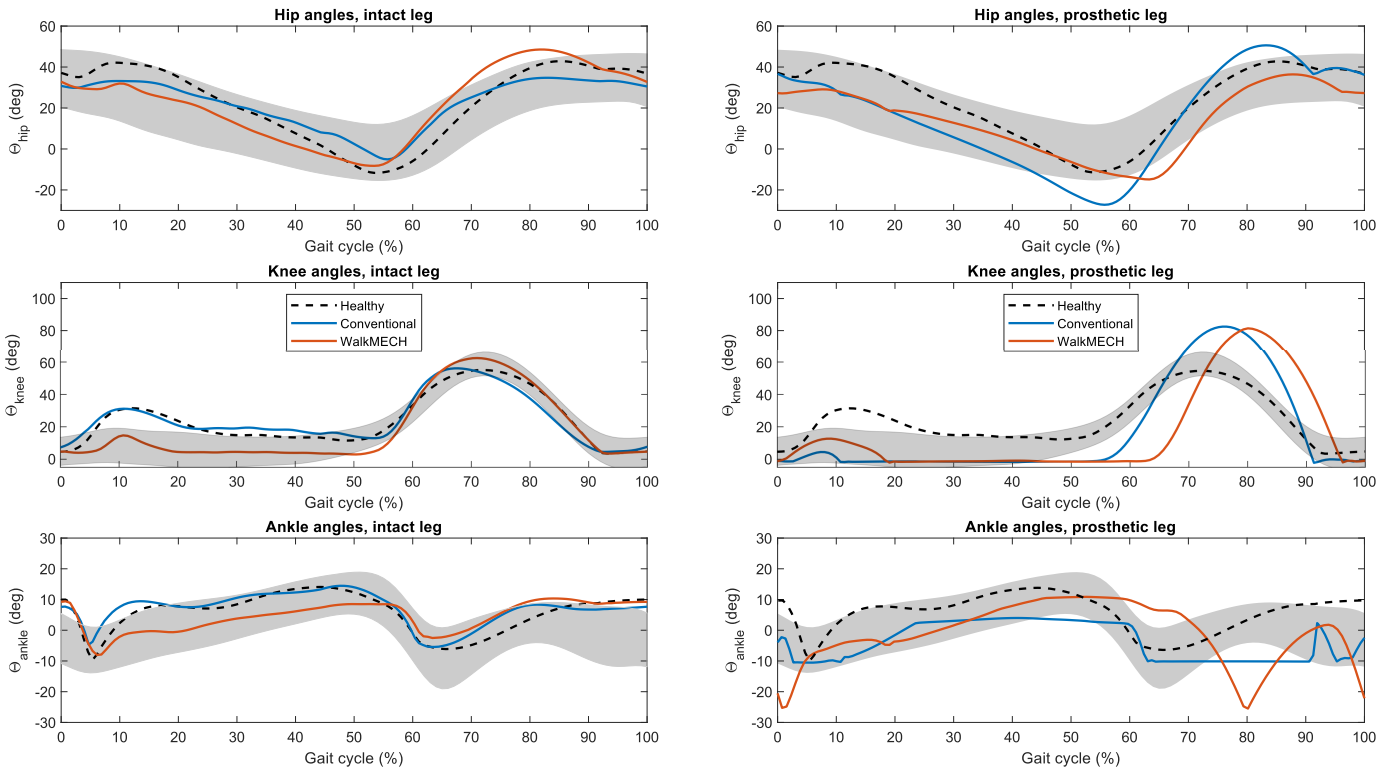

Fig 6. Joint angles. Joint angles for the three main models: HM, CM and WM. The grey bands represent experimental reference data from healthy persons walking between 0.8 and 1.0 m/s [35].

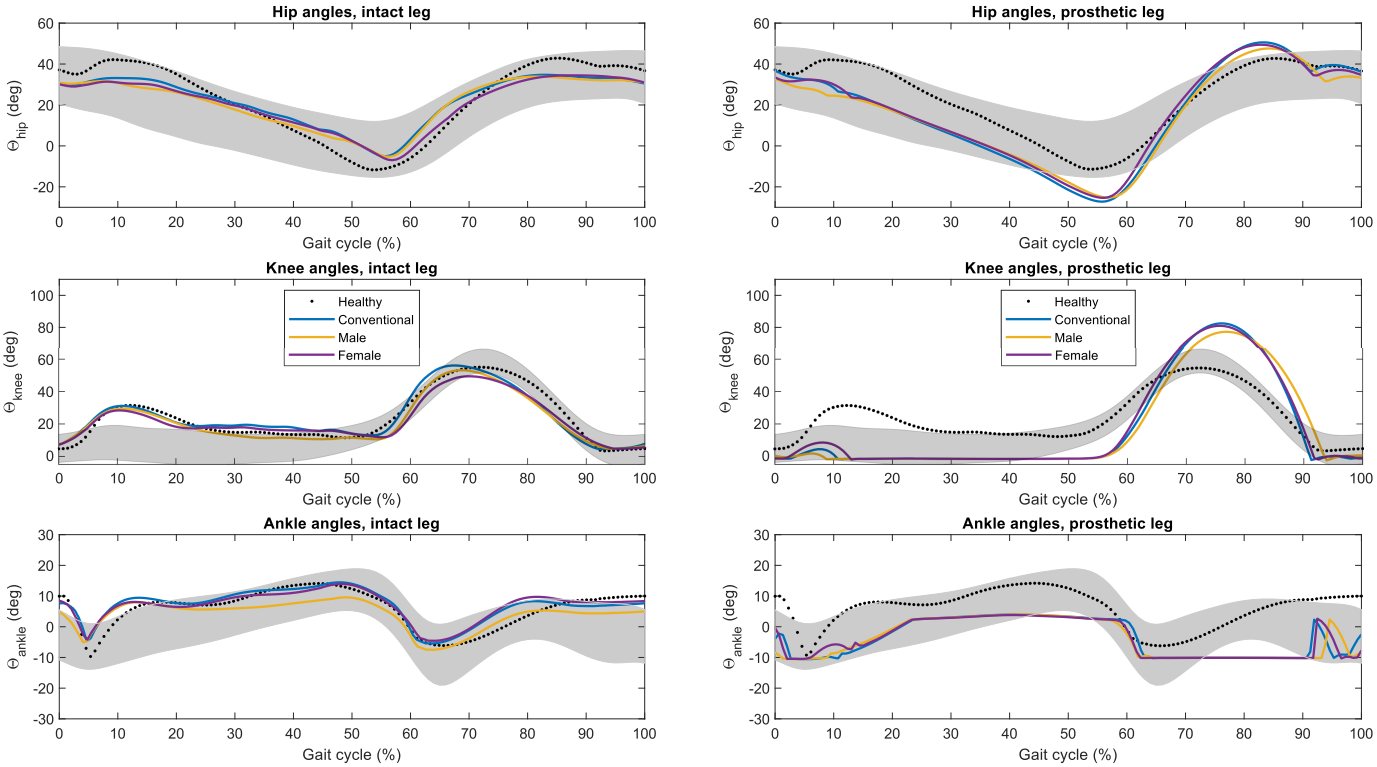

Fig 7. Conventional prosthesis joint angles. Joint angles for the conventional prosthesis model and the scaled versions: CM, CMm and CMf. The grey bands represent experimental reference data from healthy persons walking between 0.8 and 1.0 m/s [35].

The knee angles of the intact leg of CM were relatively close to those of HM. The peak flexion angle during swing was a bit earlier than in HM. The intact leg knee flexion angles of CMm and CMf were only slightly lower than those of CM. For the prosthetic leg, the knee angle remained zero during most of the stance phase, with only a small flexion angle during weight acceptance. During swing, the peak flexion angle was much higher for CM than for HM. The angles of the scaled models were very similar to CM.

For CM, the intact leg ankle angles were relatively close to those of HM. The main deviation can be found in the first part of the swing phase, where the ankle goes into dorsalflexion faster. The angles are still within range of the experimental angles. Overall CMm has lower dorsalflexion angles. For the prosthetic leg, the CM ankle angles are very different from the HM angles. In general, the ankle is longer in a plantarflexion position. Despite the large difference, the angles are mostly within range of the experimental data, except during midswing.

3.2.3 WalkMECH prosthesis model

All joint angles for WM and its variations can be found in Fig. 6 and 8. The intact leg hip angles of WM and WMb deviated from the HM angles throughout the complete gait cycle. For WMf and WMr, the hip angles were closer to HM during midstance and late stance compared to WM. For the prosthetic leg, the angles were smaller during both stance and swing. The peak angle at push-off was a bit delayed, suggesting a relatively short swing phase. This was more so the case for WM and WMb than for WMf and WMr. Because the swing phase of the intact leg seems equal for WM and HM, the double stance phase is likely longer for WM. For all variations, the peak hip angle during push-off was larger than that of HM.

The intact leg knee angles of WM were much smaller than those of HM during stance. During

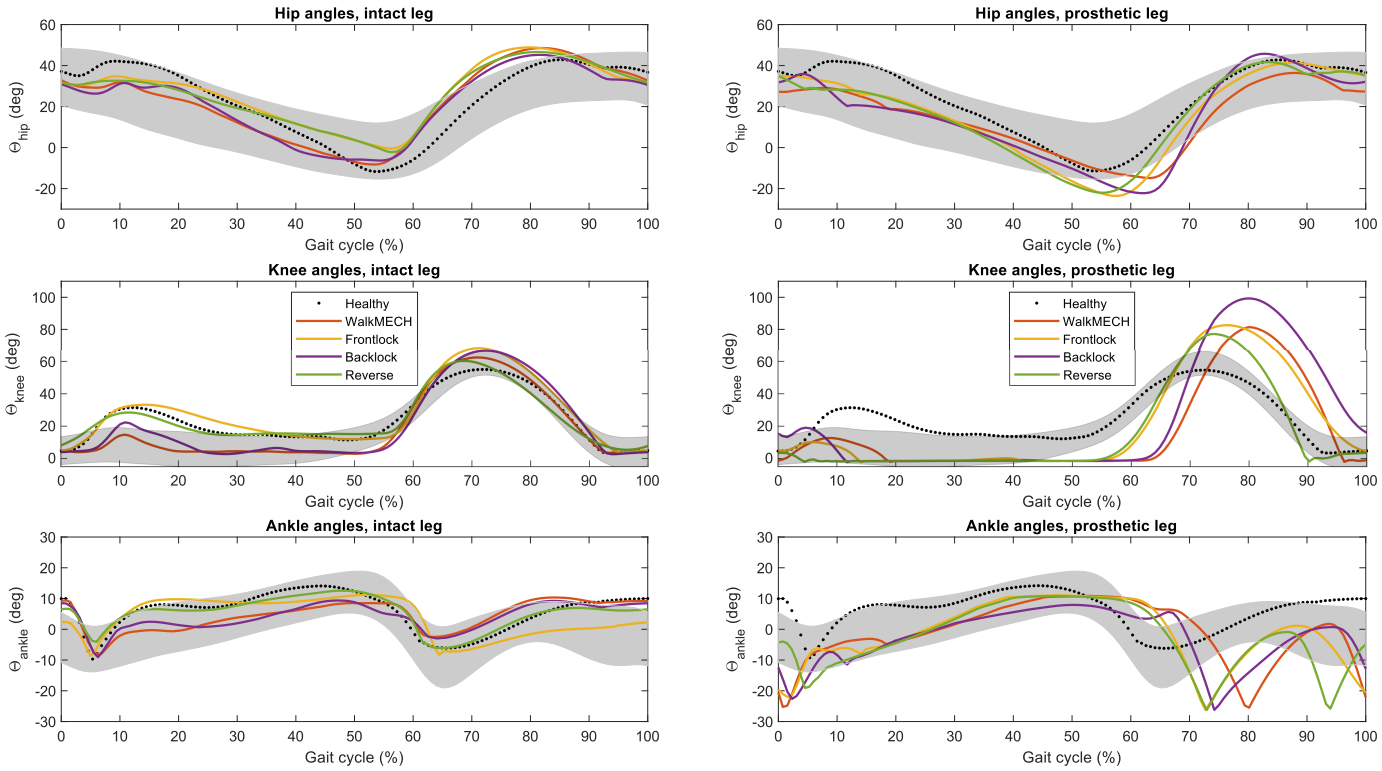

Fig 8. WalkMECH prosthesis joint angles. Joint angles for the walkMECH prosthesis model and the three variations: WM, WMf, WMb and WMr. The grey bands represent experimental reference data from healthy persons walking between 0.8 and 1.0 m/s [35].

swing, the flexion angle of WM was larger than that of HM. The knee angles were in range of the experimental data for most of the gait cycle. The angles of WMf and WMr were closer to the angles of HM. For WMr, the flexion angle deceased earlier in the swing phase, suggesting a relatively quick forward swing of the leg. However, this can not be seen in the hip and ankle angles. For the prosthetic leg, the knee angles were zero during stance for all walkMECH variations. Knee flexion started later and the peak flexion angle was much larger than HM, comparable to CM. The knee angle of WMb was larger during weight acceptance and swing. The timing of the peak knee flexion was again closer to that of HM for WMf and WMr.

The intact leg ankle angles were generally lower during stance and higher during swing. Again, they were still in range of the experimental data during stance and the start of the swing phase. However, they were slightly out of range during late swing. For WMf and WMr, the ankle angles were closer to those of HM than WM was. The angles of WMb were similar to those of WM. The ankle angles of the prosthetic leg were very different from HM. During stance, the ankle was more in plantarflexion, while in the push-off phase, there was more dorsalflexion. The plantarflexion angle during weight acceptance were smaller for WMb and WMr than those of WM and WMf. There was little difference between the ankle angles of the variations during stance. During the swing phase, the peak angles for WMf and WMr were earlier. The peak angle of WMb was also earlier, but not as much as the other two models. Overall, the plantarflexion angle during swing might be problematic for the foot clearance. Similar to what was the case for CM, there was some compensation present from the increased knee flexion angle during swing.

3.3 Ground reaction forces

3.3.1 Healthy model

In Fig. 9, it can be seen that the GRF of HM roughly follows the generally known shape of a normal GRF curve [26]. However, there are some irregularities. Just after heel strike, there is a short spike in force visible. This is due to a short bounce of the foot before the weight is fully accepted by the leg. Furthermore, the second large peak is divided in two maximums.

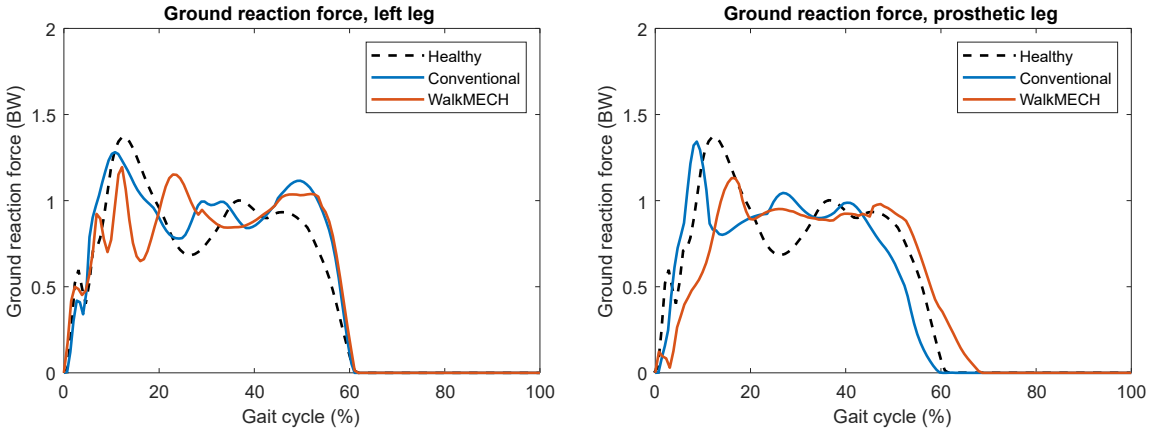

Fig 9. Ground reaction force. Ground reaction force for the three main models: HM, CM and WM.

3.3.2 Conventional prosthesis model

The maximum GRF of the intact leg of CM was lower than that of HM (see Fig. 9). Although the general shape of the curve was similar, the peak for push-off was higher and delayed. The GRF of CMf was very similar to CM, but was slightly higher at the weight acceptance and push-off peaks (see Fig. 10). The GRF of CMm had an even higher peak of weight acceptance, but a peak equally high to that of CM for push-off. The dip in between the two peaks is also less deep for CMm.

The weight acceptance peak of the prosthetic leg took place earlier in the gait cycle and was narrower than that of HM. The peak for push-off was again slightly higher, and also shifted forward. This shows that the stance phase of the prosthetic leg was just slightly shorter, and that the push-off was longer. The CM variations had equal GRF curves for push-off, but were significantly different for weight acceptance. The peak force of both CMm and CMf was lower, while the dip after weight acceptance was also way lower than that of the other two models for CMf. Overall, the GRF curves for CM and its variations are notably more irregular than those of HM.

3.3.3 WalkMECH prosthesis model

The maximum GRF of both legs was lower for WM than for both CM and HM (see Fig. 9). The peaks were much more irregular and no clear pattern can be discovered. The stance phase of the intact leg was as long as for HM and CM.

However, the stance phase of the prosthetic leg was significantly longer for WM. This is in line with what was found in the joint angles and loads. For WMb, there was a large bounce during weight acceptance, visible as a peak and large dip before the main peak. The stance phase of WM and WMb were equally long. The stance phase of both WMf and WMr were shorter, approaching the stance phase length of HM. The peak force at weight acceptance was also more like HM for these two variations. The height op the peaks at push-off was approximately equal for all models, with a slightly larger peak for WMb.

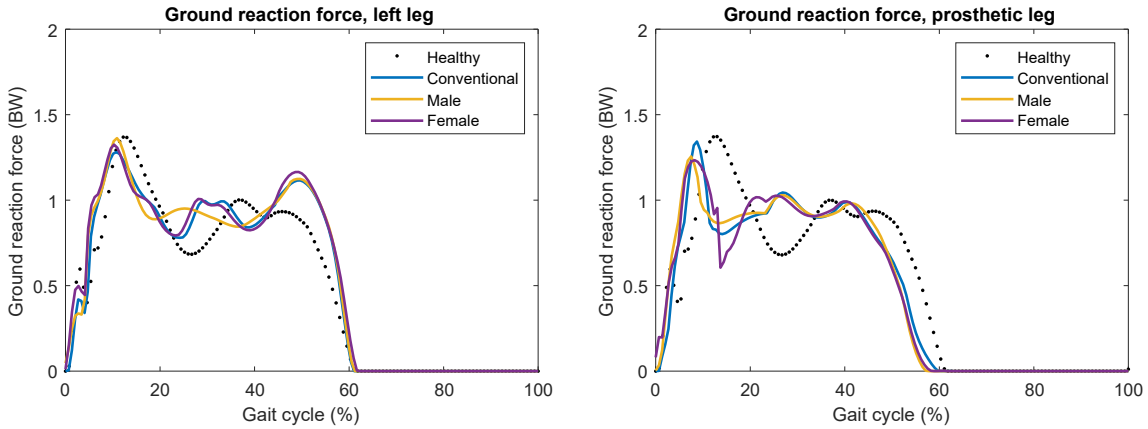

Fig 10. Conventional prosthesis ground reaction force. Ground reaction force for the conventional prosthesis model and its variations: CM, CMm and CMf.

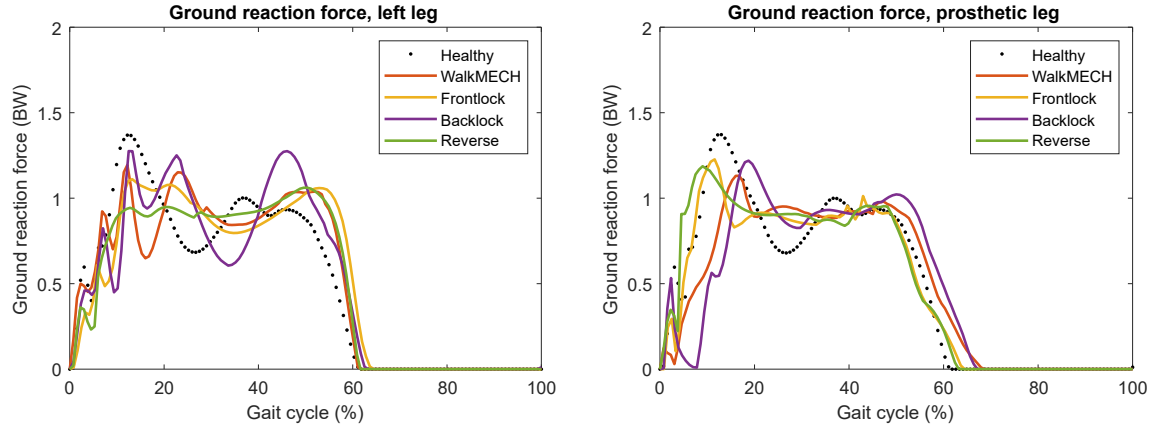

Fig 11. WalkMECH prosthesis ground reaction force. Ground reaction force for the walkMECH prosthesis model and its variations: WM, WMf, WMb and WMr.

3.4 Muscle activation

3.4.1 Healthy model

The muscle activation of HM can be found in Fig. 13. Reference EMG data were taken from Cappellini et al. [36], from which the relevant graphs can be found in Fig. 12. Some of the muscles cannot be compared one-on-one. No experimental data were reported for the activation pattern of the biceps femoris short head. The hamstrings are composed of three muscles, of which the biceps femoris long head and the semitendinosus are reported separately in the reference data. The same is true for the vasti and the gastrocnemius, of which the medial and lateral part are reported separately. It should be noted that the muscle activation data from the optimisations are reported with respect to the maximum activation of the respective muscle (0-1), whereas the experimental EMG data are reported in µV (0-50µV). The comparison should therefore be made based on the shape of the activation curve, and not based on the absolute height.

For the hamstrings, only the activation at the start of the stance phase is present in HM. The activation at the end of swing in the reference data is not present in HM. The same is true for the gluteus maximus. However, the activation at late swing in the experimental data is very low, making the difference smaller. For both the gluteus maximus and hamstrings, the activation in early- to midstance might be too high compared to the experimental data. While the shape of the activation curve for the iliopsoas seems to be very similar for the simulation and experimental data, the height

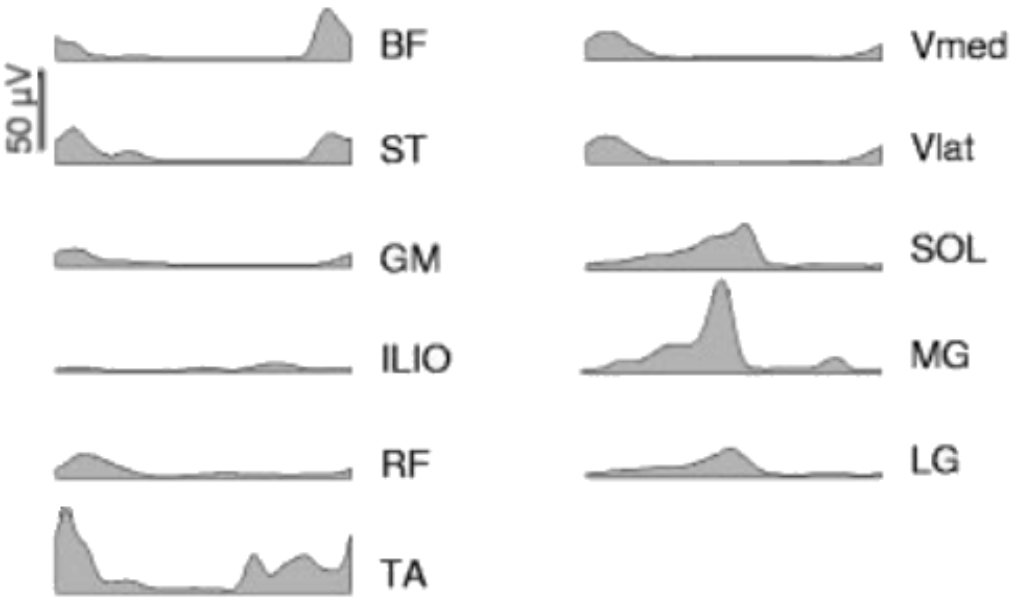

Fig 12. Reference data for muscle activation. Experimental data for muscle activation of healthy gait. The simulation results compare to the experimental data (sim:exp) as follows: hamstrings: BF (biceps femoris, long head) and ST (semitendinosus), gluteus maximus: GM, iliopsoas: ILIO, rectus femoris: RF, biceps femoralis short head:not available, vasti: Vmed and Vlat (medial and lateral vastus), gastrocnemius: MG and LG (medial and lateral gastrocnemius), soleus: SOL, tibialis anterior: TA. The experimental data were taken and adapted from Cappellini et al. [36].

of the activation might be too high in the simulations. For the rectus femoris, there is barely any activation in HM, while there is a significant amount of activation during loading response in the experimental data. The activation pattern for the vasti is approximately equal for HM and the experimental data. However, the vasti are active for a larger part of the stance phase in HM. The activation pattern of the soleus also seems to be very similar for both data sets. The gastrocnemius is activated at the same time for both data sets. However, the relative activation difference is larger in the experimental data (e.g. there is a higher sudden peak). The same is seems to be true for the tibialis anterior.

3.4.2 Conventional prosthesis model

As can be seen in Fig. 13, the activation of the left hamstrings starts later than in HM. The maximum activation is also lower for CM than for HM. In CMm, the activation starts even later than in CM (see Fig. 14). The amount of activation of the hamstrings is equal for CM, CMm and CMf. The hamstrings of the prosthetic side are activated earlier and more than in HM.

The intact leg gluteus maximus of CM was activated less and shorter than those in HM. For CMf, the muscle was activated less than for CM. The gluteus maximus was barely activated for CMm. Again, the gluteus maximus of the prosthetic leg were activated more and earlier than those in HM. The activation pattern is very similar to that of the hamstrings of the same leg. For CMm and CMf, the gluteus maximus was activated slightly less.

The iliopsoas of the intact leg was activated much shorter and less in CM than in HM. The activation for CMf and CMm were similar. The activation of the iliopsoas in the prosthetic leg was much more like that of HM. The maximum activation was still slightly lower than HM. For CMm and CMf, the activation was a bit lower than for CM.

For both the intact and the prosthetic leg, there was a small peak in the activation of the rectus femoris where there was barely any activation in HM. This was only the case for CM and CMm for

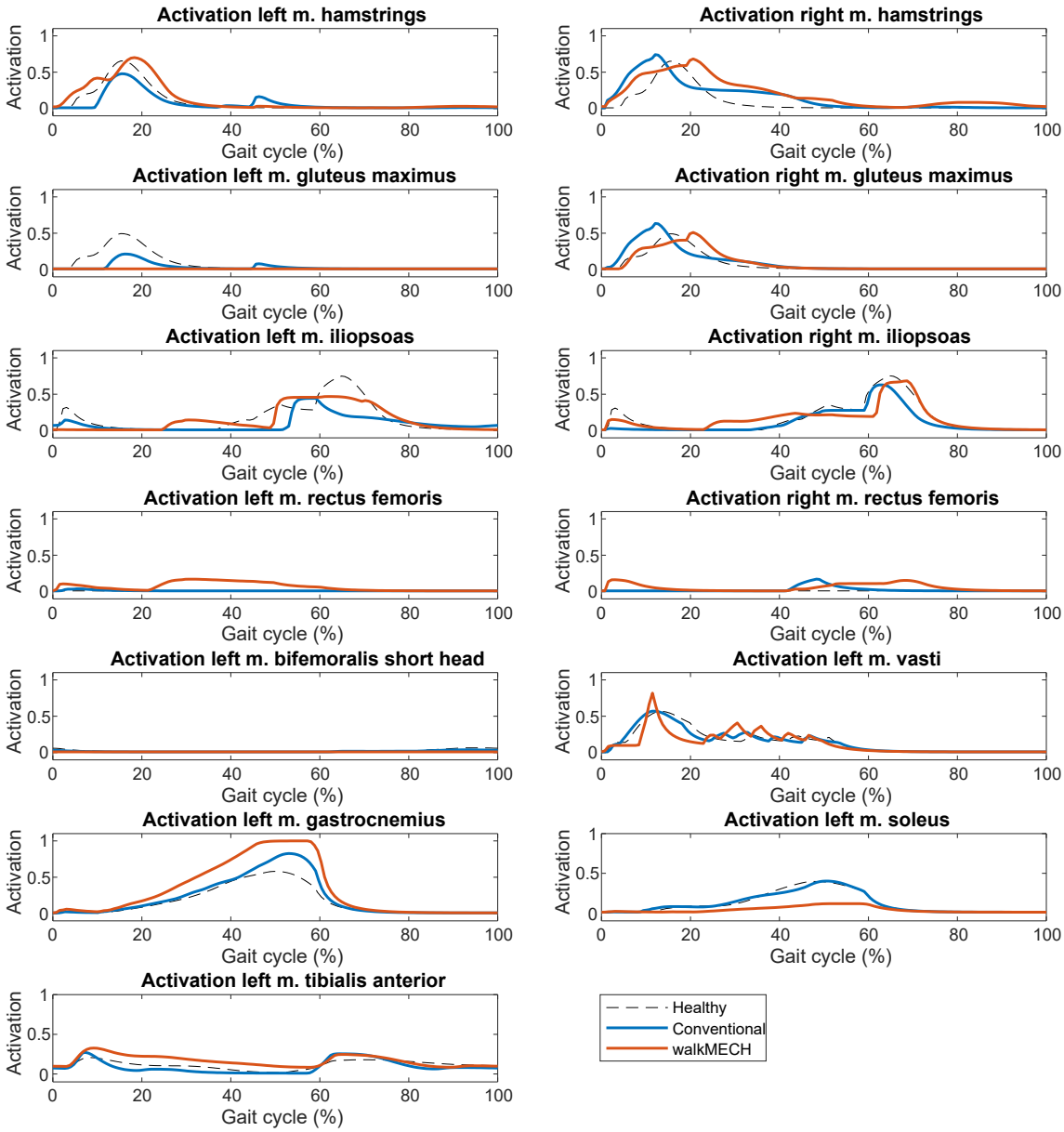

Fig 13. Muscle activation. Muscle activation for the three main models: HM, CM and WM.

the intact leg and for all variations for the prosthetic leg.

For the biceps femoris short head, there was a very small amount of activation at the end of the swing phase, similar to in HM. This muscle was only present in the intact leg of the model, as it only crosses the knee.

The vasti were activated very similar for all variations of CM and HM.

The gastrocnemius of the left leg was activated more during push-off, but equal to HM during the remainder of the gait cycle. The activation for CMm was slightly lower and the activation of CMf was as high as that of HM.

The activation of the soleus was almost equal for CM and HM. The activation for CMf was similar to that for CM, while that of CMm was lower during push-off.

For the tibialis anterior, the activation during stance and late swing was slightly lower for CM

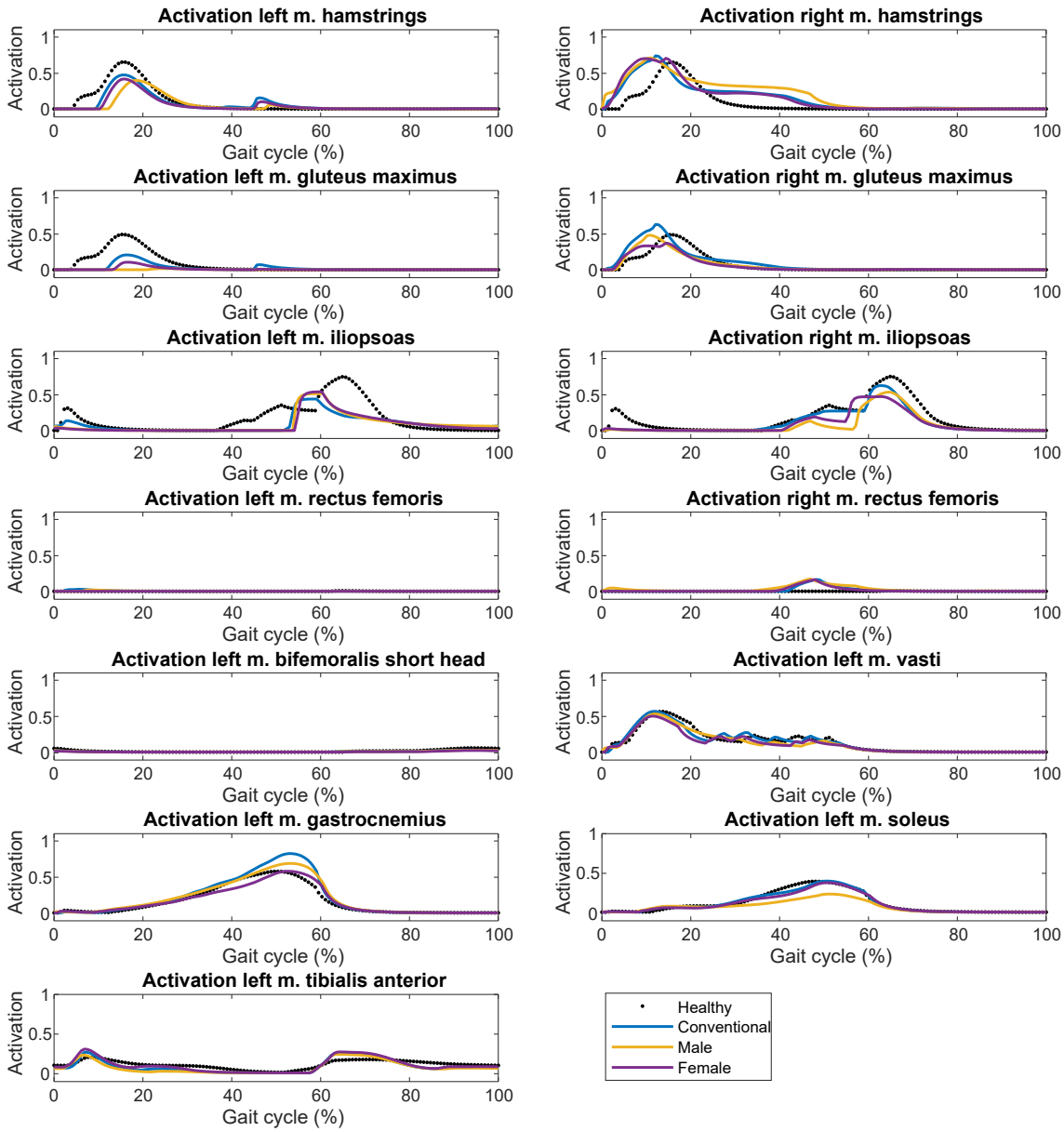

Fig 14. Conventional prosthesis muscle activation. Muscle activation for the conventional prosthesis model and its scaled models: CM, CMm and CMf.

than for HM and slightly higher during preswing. Overall, the activation of CMf was a bit higher than CM and the activation of CMm was a bit lower than CM.

3.4.3 WalkMECH prosthesis model

The activation of the both the left and right hamstrings was higher for WM than for HM. The timing of the activation was equal. For the intact leg, the activation in WMb started later, had an equal peak activation to WM. Both WMf and WMr had a lower maximum activation level for the hamstrings. Contrary to this, the activation level of the hamstrings of the prosthetic leg were much higher for WMf and WMr than for WM. The activation in WMb was slightly higher during weight acceptance and had a large peak during midswing.

The gluteus maximus of the intact leg was barely active for WM. The activation was more like that of HM for WMb and even more alike for WMr. The activation for WMf was higher than HR, but peaked later. The prosthetic side gluteus maximus was activated more like HM than CM, but peaked a bit later than HM. The gluteus maximus activation in WMb was much higher than in all other variations. For WMf and WMr, the activation was equal to that of HM for the first half of loading response. After that point, the activation level was lower than that of WM and HM.

The activation of the intact side iliopsoas started earlier than in HM, during midstance. This part of the activation pattern was higher for WMb. After that point, the activation of the iliopsoas in WMb followed that in WM. The maximum activation during swing was lower for WM than for HM. For WMf and WMr, the activation peak was much higher and took place earlier than the peak in

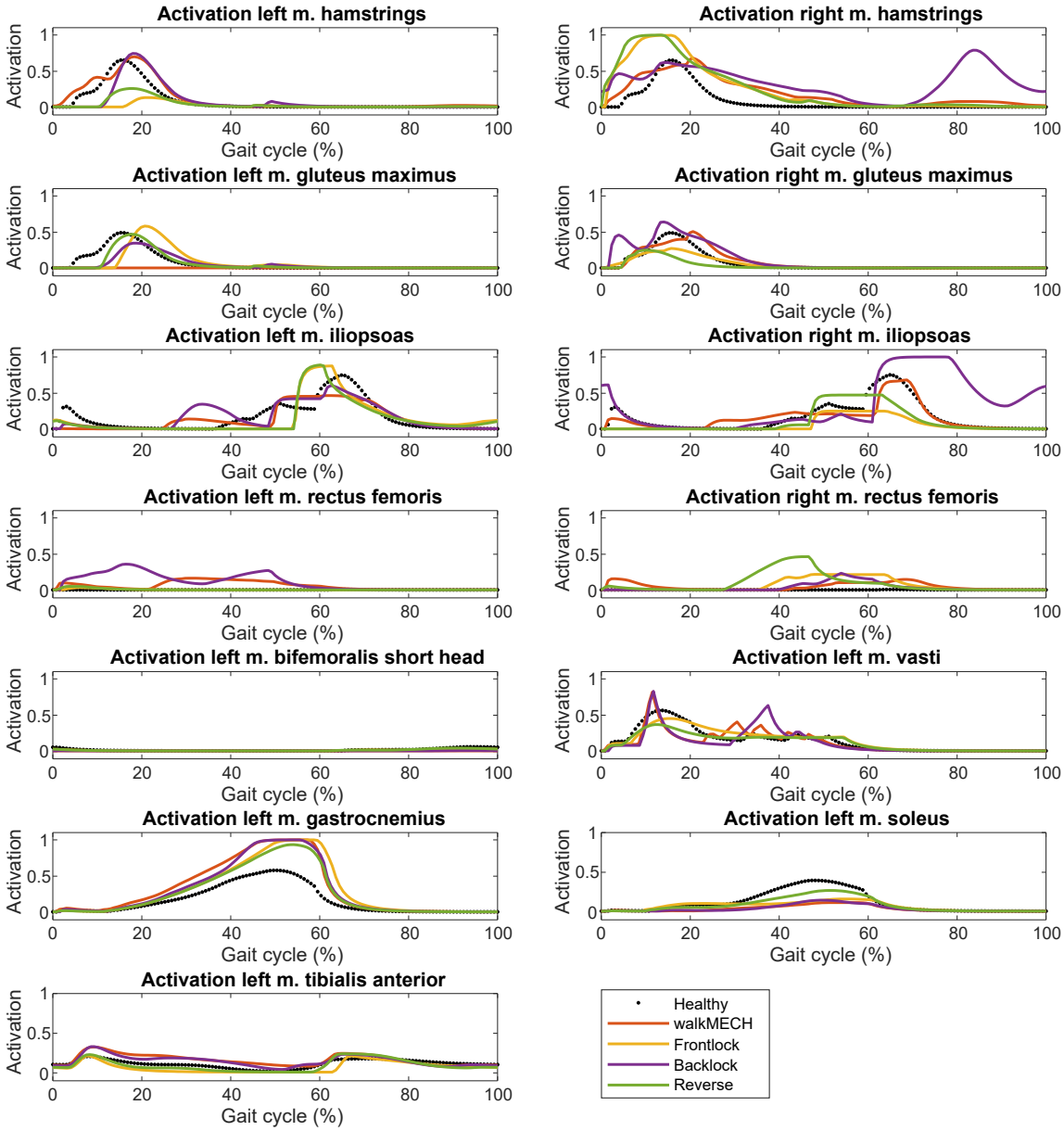

Fig 15. WalkMECH muscle activation. Muscle activation for the walkMECH model and its variations: WM, WMf, WMb and WMr.

HM. The activation pattern of WM in the prosthetic leg was more similar to that of HM. Although the activation during stance was slightly higher, the overall shape was closer to a healthy pattern. For WMr, the activation was higher during push-off, but lower during swing. This was also the case for WMf, but with an even lower level. The activation of WMb was lower during push-off, and much higher during swing. The peak activation was significantly higher for WMb than for any of the other variations and HM.

For the rectus femoris of WM, there was a little activation during mid- to terminal stance, while there was none for HM. The activation for WMf and WMr were close to zero and therefore similar to that of HM. WMb had a relatively high activation during the whole stance phase. The rectus femoris in the prosthetic leg of WM was activated during heel strike and around push-off. The activation during push-off was similar, but slightly higher for WMb and a little higher for WMf. The activation for WMr was much higher at heel off and started earlier as well.

The biceps femoris short head was barely activated for all variations and was therefore very similar to that in HM. WMb showed the same activation pattern during loading response, but had one higher peak between midstance and heel-off, where WM had only one. The activation pattern for WMf and WMr was much more similar to HM.

The activation pattern of WM for the vasti globally followed the curve of that of HM, but was much more irregular. The activation curve was irregular, with the maximum activation being higher than the maximum activation for HM.

The activation of the gastrocnemius was much higher for WM than for both CM and HM. It is remarkable that the activation during push-off seems to reach the maximum value and plateaus, while the activation in HM only reaches half of the amount of activation. While the activation in WMb was very similar, the activation in WMf and WMr was only slightly lower. The opposite was true for the activation of the soleus. While there was much less activation for WM, WMf and WMb than for HM, the activation level for WMr was more like that of HM.

The peak activation of the tibialis anterior was higher for WM than for HM, but the activation pattern was equal. The same was true for the activation in WMb. The activation for WMf and WMr was lower, to the point that is was even lower than HM during midstance and toe-off.

In general, the muscle activation of the different models are difficult to compare and interpret. This is more so the case for the variations on the walkMECH.

4 Discussion

The purpose of this study was to gain insight into transfemoral prosthesis design through musculoskeletal modelling and predictive simulations. This section discusses the results that were found and their implications for the application of the studied methods. The limitations of and opportunities for the methods will also be discussed.

4.1 Results interpretation

We found that the CoT for walking was less energetically expensive than walking with a healthy body. Because there is extensive proof that the opposite is true, these results can not be considered reliable [7, 22]. One possible explanation is that a musculoskeletal model lacks some of the properties of an actual human being. An aspect that cannot be simulated is fear of falling. An amputee patient will most likely use cocontraction to stabilise the body and reduce the risk of falling. Cocontraction can take up a large amount of energy [37].

Furthermore, not all muscles present in the body were included in the models. Including all muscles in the model would make it more difficult and time costly to simulate. For the purpose of this thesis, it was chosen to simplify the model to a more basic form including only the most important leg muscles. This might also be the cause for inconsistent results for muscle activation. While some of the more prominent activation patterns were similar between simulation results and experimental data, many irregularities and deviations were found. These are difficult to interpret

and do not seem to account for the inaccuracy of the CoT found. Considering the cumulative amount of activation, it can not be concluded that the models with an overall lower amount of activation were also the models with a lower CoT.

The activation of the gastrocnemius in WM was higher than in CM, which was higher than in HM. Given this large difference, it might be concluded that a considerably higher amount of push-off power was generated by the intact leg of CM, and even more so in WM. This conclusion is drawn with the assumption that there is some accuracy in the muscle activation found. The higher amount of push-off generated could be caused by the need of compensation for lack of push-off in the prosthetic leg.

The high amount of push-off in the intact leg can also be seen in the GRF. The peak GRF of both CM and WM was higher than HM during push off. However, the difference between CM and WM was very small, contradicting the large difference in gastrocnemius activation between the two models. Surprisingly, the amount of push-off that can be seen in the GRF of the prosthetic leg is not lower than of the same leg in HM. This suggests that the expectations about the push-off being lower for prosthetic models would not be true. It should be noted that the GRF during midstance was approximately as high as during push-off for the prosthetic models. This does imply a lack of push-off, which is contrary to the conclusion drawn from comparison between HM, CM and WM.

Overall, the GRF was very irregular for most models. This might indicate that a optimal solution was not reached.

The lack of push-off through ankle plantarflexion can be found in the joint angles resulting from the simulations. For CM, there was only a small difference in ankle angle during push-off. For WM, the ankle plantarflexion was significantly delayed. When comparing the timing of plantarflexion with the GRF data, it can be concluded that the plantarflexion does start at the end of push-off. However, a significant amount of plantarflexion is reached well after the foot has lost contact with the ground.

The kinematic data of the prosthetic leg also show that the extreme angles of the hip and knee were significantly larger than for HM. The increase in hip flexion and extension in CM could be the result of a larger step size. This is confirmed by the values found and reported in Table 3. The shorter stride length in WM likely causes the smaller hip flexion angle found for the prosthetic leg.

The increased knee angle for both prosthetic legs might be a compensation strategy to increase the amount of foot clearance. The difference in intact leg kinematics are not too large.

In both the GRF and joint kinematics of the prosthetic leg of WM, it can be seen that the stance phase to swing phase ratio is shifted with respect to both other models. The stance phase was considerably longer for WM.

For the scaled CM models, all results were very similar to the base model. This is conform expectations. It also suggests that when scaled accordingly, a prosthesis can function equal for persons with different anthropometry.

The results for the WM variations were very irregular. We therefore have low confidence that the predictive simulations converged to the global minimum for these models. The following conclusions are very uncertain. The results for the variation in which the slider was locked in the back of the slot were most similar to those of the WM itself. This is true to expectations, since in WM, the slider is located in the back of the slot for most of the gait cycle.

The joint kinematics of the WM variations show that for WMf and WMr, the stance- to swing phase ratio was more normal. The ankle plantarflexion of the prosthetic leg also took place earlier in the gait cycle, but still does not seem to contribute to push-off very much, nor does it contribute less. This effect was not expected, since the walkMECH was designed to provide support in the push-off phase and should therefore perform better than its variations.

The muscle activation of the prosthetic leg of WM variations was remarkably high in some places and very varied. No conclusions can be drawn from these results at all.

4.2 Limitations

The first issue that needs to be addressed is the large difference in CoT between the results of this paper and that of Ong et al. [22]. It would be good to find out what the cause is of this difference

and whether the prosthetic models can also be run with the model and simulation method of Ong et al. [22]. Attempts to remedy this issue were not fruitful within the time spent. Because of time restrictions, this path was not investigated further and was left for future research.

It is suspected that not all, if any, of the predictive simulations reached the global minimum. More simulations need to be done with a wider range of initial conditions to try to find the global minimum.

In the GRF results, it became apparent that all models had a small bounce of the foot at heel strike. Since this bounce is not present in a normal gait pattern, it should be attempted to remove it. It is expected that the problem can be overcome by fine-tuning the contact properties between the foot contact spheres and the ground.

Lastly, the slider movement of the walkMECH was found to be slightly different from the movement reported by Unal et al. [14]. The slider and blocking system were attempted to be modelled correctly via two methods, of which the best was used in this study. It should be attempted to find a better method or better settings of the current method in order to further improve the slider movement.

4.3 Recommendations

Before further research can be done, the existing issues and uncertainties must be addressed and solved. If these changes to lead to more realistic results, our confidence in the models created by us would increase.

In future studies, it is recommended to test the modelling and simulation of a wider range of prostheses and prosthetic components. This should be done in order to investigate the effect of these components on the gait pattern and to see whether the investigated methods are also reliable for other mechanical components than those tested. Some of the main components that need to be tested are hydraulic and pneumatic cylinders and active actuation of joints in combination with different motion sensors (feedback) or pre-programmed motions.

In order to better validate the design methods, a model should be created that is scaled to a specific person and specific prosthesis. Results should then be gathered through both simulations and experiments, aimed at the same outcome measures. Only through comparison of these data can be found whether musculoskeletal models and predictive simulations can be an accurate tool for design purposes.

5 Conclusion

Because we do not have confidence that realistic results and optimal solutions for the optimisation problem were reached in all models, we can not formulate inconclusive conclusions. OpenSim and SCONE allow for the facile creation of prosthesis design models. However, the effect of the prosthesis design on gait properties like CoT is still uncertain.

6 Acknowledgments

The creation of this study would not have been possible without my supervisor, Ajay Seth. Nor would it without Thomas Geijtenbeek and Gerwin Smit, who have invested time and expertise to help me. I would also like to thank Ramazan Unal and Omid Khosrowshahi, who have answered all my questions about the walkMECH and made it possible to model it. Furthermore, I would like to thank Jacqueline, who was available for discussions and ideas. Lastly, I would like to thank my parents and partner for the endless support throughout this journey.

References

1. Hughes W, Goodall R, Salciccioli JD, Marshall DC, Davies AH, Shalhoub J. Editor's Choice–Trends in lower extremity amputation incidence in European Union 15+ countries 1990–2017. European Journal of Vascular and Endovascular Surgery. 2020;60(4):602–612.

2. Ziegler-Graham K, Mackenzie E, Ephraim P, Travison T, Brookmeyer R. Estimating the Prevalence of Limb Loss in the United States: 2005 to 2050. Archives of physical medicine and rehabilitation. 2008;89:422–9. doi:10.1016/j.apmr.2007.11.005.

3. Passel J, Cohn D, Center P. U.S. Population Projections: 2005-2050. Pew Research Center; 2008.

4. George J, Navale S, Nageeb E, Curtis G, Klika A, Barsoum W, et al. Etiology of Above-knee Amputations in the United States: Is Periprosthetic Joint Infection an Emerging Cause? Clinical Orthopaedics and Related Research. 2018;476:1. doi:10.1007/s11999.0000000000000166.

5. Gurney J, Stanley J, Rosenbaum D, Sarfati D. Risk of lower limb amputation in a national prevalent cohort of patients with diabetes. Diabetologia. 2018;61. doi:10.1007/s00125-017-4488-8.

6. Gjøvaag T, Starholm IM, Mirtaheri P, Hegge F, Skjetne K. Assessment of aerobic capacity and walking economy of unilateral transfemoral amputees. Prosthetics and orthotics international. 2013;38. doi:10.1177/0309364613490444.

7. Wong C, Benoy S, Blackwell W, Jones S, Rahal R. Systematic review of energy consumption in microprocessor knee prosthesis users compared to non-microprocessor knee prosthesis users. JPO Journal of Prosthetics and Orthotics. 2012;24:202–8. doi:10.1097/JPO.0b013e31826f5e51.

8. Kaufman K, Levine J, Brey R, Mccrady S, Padgett D, Joyner M. Energy Expenditure and Activity of Transfemoral Amputees Using Mechanical and Microprocessor-Controlled Prosthetic Knees. Archives of physical medicine and rehabilitation. 2008;89:1380–5. doi:10.1016/j.apmr.2007.11.053.

9. Bock O. Otto Bock prostheses; n.d. Available from: `https://www.ottobock.nl/prothesen/`.

10. US OB. Otto Bock Pricelist; 2018. Available from: `https://shop.ottobock.us/media/pdf/14503_US_2018_PriceList.pdf`.

11. Cherelle P, Mathijssen G, Wang Q, Vanderborght B, Lefeber D. Review Article Advances in Propulsive Bionic Feet and Their Actuation Principles. Advances in Mechanical Engineering. 2014;2014:1–22. doi:10.1155/2014/984046.

12. Houdijk H, Wezenberg D, Hak L, Cutti A. Energy storing and return prosthetic feet improve step length symmetry while preserving margins of stability in persons with transtibial amputation. Journal of NeuroEngineering and Rehabilitation. 2018;15. doi:10.1186/s12984-018-0404-9.

13. Blatchford. Linx - Blatchford - Mobility Made Possible; 2020. Available from: `https://www.blatchford.co.uk/products/linx/`.

14. Unal R, Behrens SM, Carloni R, Hekman EEG, Stramigioli S, Koopman B. Conceptual Design of a Fully Passive Transfemoral Prosthesis to Facilitate Energy-Efficient Gait. IEEE Transactions on Neural Systems and Rehabilitation Engineering. 2018;PP:1–1. doi:10.1109/TNSRE.2018.2880345.

15. Sup IV F, Varol A, Goldfarb M. Upslope Walking With a Powered Knee and Ankle Prosthesis: Initial Results With an Amputee Subject. IEEE transactions on neural systems and rehabilitation engineering : a publication of the IEEE Engineering in Medicine and Biology Society. 2010;19:71–8. doi:10.1109/TNSRE.2010.2087360.

16. Quintero Maldonado D, Villarreal D, Lambert D, Kapp S, Gregg R. Continuous-Phase Control of a Powered Knee–Ankle Prosthesis: Amputee Experiments Across Speeds and Inclines. IEEE Transactions on Robotics. 2018;PP:1–16. doi:10.1109/TRO.2018.2794536.

17. Lee JW, Daly S, Huang-Saad A, Seifert C. Start With Problems or Solutions? Medical Device Design in Industry and Academia. IEEE Access. 2020;8:208623–208642. doi:10.1109/ACCESS.2020.3035966.

18. Seth A, Hicks J, Uchida T, Habib A, Dembia C, Dunne J, et al. OpenSim: Simulating musculoskeletal dynamics and neuromuscular control to study human and animal movement. PLOS Computational Biology. 2018;14:e1006223. doi:10.1371/journal.pcbi.1006223.

19. Delp S, Anderson F, Arnold A, Loan P, Habib A, John C, et al. OpenSim: Open-Source Software to Create and Analyze Dynamic Simulations of Movement. Biomedical Engineering, IEEE Transactions on. 2007;54:1940 – 1950. doi:10.1109/TBME.2007.901024.

20. Geijtenbeek T. SCONE: Open Source Software for Predictive Simulation of Biological Motion. Journal of Open Source Software. 2019;4:1421. doi:10.21105/joss.01421.

21. Ong CF, Geijtenbeek T, Hicks JL, Delp SL. Predictive simulations of human walking produce realistic cost of transport at a range of speeds. In: Proceedings of the 16th International Symposium on Computer Simulation in Biomechanics; 2017. p. 19–20. Available from: `http://resolver.tudelft.nl/uuid:bd24be48-eb8e-4934-9157-82685d439eeb`.

22. Ong C, Geijtenbeek T, Hicks J, Delp S. Predicting gait adaptations due to ankle plantarflexor muscle weakness and contracture using physics-based musculoskeletal simulations. PLOS Computational Biology. 2019;15:e1006993. doi:10.1371/journal.pcbi.1006993.

23. LaPre A, Price M, Wedge R, Umberger BR, Sup IV F. Approach for Gait Analysis in Persons with Limb Loss Including Residuum and Prosthesis Socket Dynamics. International Journal for Numerical Methods in Biomedical Engineering. 2017;34:e2936. doi:10.1002/cnm.2936.

24. Boonstra A, Schrama J, Fidler V, Eisma W. Energy cost during ambulation in transfemoral amputees: a knee joint with a mechanical swing phase control vs a knee joint with a pneumatic swing phase control. Scandinavian journal of rehabilitation medicine. 1995;27(2):77–82.

25. Boonstra A, Schrama J, Eisma W, Hof A, Fidler V. Gait analysis of transfemoral amputee patients using prostheses with two different knee joints. Archives of physical medicine and rehabilitation. 1996;77(5):515–520.

26. Winter D. Kinematic and kinetic patterns in human gait: Variability and compensating effects. Human Movement Science - HUM MOVEMENT SCI. 1984;3:51–76. doi:10.1016/0167-9457(84)90005-8.

27. Plagenhoef S, Evans F, Abdelnour T. Anatomical Data for Analyzing Human Motion. Research Quarterly for Exercise and Sport. 2013;54:169–178. doi:10.1080/02701367.1983.10605290.

28. Hansen N. The CMA evolution strategy: A tutorial. arXiv preprint arXiv:160400772. 2016;.

29. Alho A, Høiseth A, Husby T. Bone-mass distribution in the femur A cadaver study on the relations of structure and strength. Acta orthopaedica Scandinavica. 1989;60:101–4. doi:10.3109/17453678909150104.

30. Lieber R. Skeletal muscle structure, function, and plasticity. Lippincott Williams And Wilkins; 2011.

31. Hunt KH, Crossley FRE. Coefficient of restitution interpreted as damping in vibroimpact. Journal of Applied Mechanics. 1975;42(2):440–445. doi:10.1115/1.3423596.

32. Koopman HFJM, Behrens SM, Carloni R, Hekman EEG, Stramigioli S, Ünal R, et al., inventors; A prosthetic or orthotic device. WO2012177125A1; 2012. Available from: https://patentimages.storage.googleapis.com/5d/15/89/5e494e182f1be0/WO2012177125A1.pdf.

33. Uchida TK, Hicks JL, Dembia CL, Delp SL. Stretching your energetic budget: how tendon compliance affects the metabolic cost of running. PloS one. 2016;11(3):e0150378.

34. Geijtenbeek T. Documentation [SCONE]; 2019. Available from: https://scone.software/doku.php?id=doc%3Astart.

35. Mentiplay B, Banky M, Clark R, Kahn M, Williams G. Lower limb angular velocity during walking at various speeds. Gait & Posture. 2018;65. doi:10.1016/j.gaitpost.2018.06.162.

36. Cappellini G, Ivanenko Y, Poppele R, Lacquaniti F. Motor Patterns in Human Walking and Running. Journal of neurophysiology. 2006;95:3426–37. doi:10.1152/jn.00081.2006.

37. Unnithan VB, Dowling JJ, Frost G, Bar-Or O. Role of cocontraction in the O2 cost of walking in children with cerebral palsy. Medicine and science in sports and exercise. 1996;28(12):1498–1504.

38. Community BO. Blender - a 3D modelling and rendering package; 2018. Available from: http://www.blender.org.

39. Vallery H, Schwab AL, (Delft) TU. Advanced Dynamics. Delft University of Technology; 2017. Available from: https://books.google.nl/books?id=gUd8tgEACAAJ.

40. Heidari B. Knee osteoarthritis prevalence, risk factors, pathogenesis and features: Part I. Caspian journal of internal medicine. 2011;2(2):205.

A Appendix

A.1 Femur mass

The mass of the shortened femur (see Fig. 16) was calculated based on the data found by Alho, Høiseth and Husby [29], which can be found in Table 4. To keep the model as general as possible, the mean masses of the male and female participants were combined. In the model, approximately 15 cm of distal end of the femur was removed. This corresponds to about 10 cm of the shaft and the complete condyles, which weight a total of $2.4974 * \frac{10}{34} + 2.6170 = 3.3515$ kg. The remaining mass of the amputated femur was therefore set to 5.9500 kg. In the model, the femur has the mass of the total thigh. In these calculations, it is assumed that the mass distribution of the femur can be extrapolated to the mass distribution of the thigh.

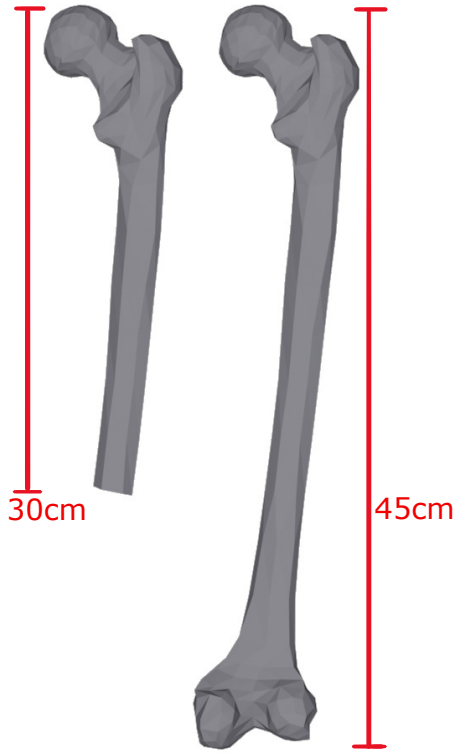

Fig 16. Trans-section of the femur. Original model from the OpenSim database [18, 19]. Edited in Blender [38].

Table 4. Mass of individual sections of the femur. Mean absolute masses originate from Alho, Høiseth and Husby [29] (density (HU) x volume (cm^3)). Total mass of femur is standard mass in OpenSim database.

	Male		Female		All	
	Mean absolute mass	Relative mass	Mean absolute mass	Relative mass	Relative mass	Absolute mass (kg)
Head	6140	22.1%	4380	22%	22.05%	2.0510
Neck	6220	22.4%	4710	23.7%	23.05%	2.1440
Shaft	6900	24.9%	5720	28.7%	26.8%	2.4974
Condyles	8480	30.6%	5090	25.6%	28.1%	2.6170
Total	27740	100%	1990	100%	100%	9.3014

A.2 Inertia calculations

The inertia of all anatomic components of the model were preexisting and did not need to be recalculated. However, the inertia of all prosthetic components was not reported in the articles in which they were described. Therefore, these were calculated based on basic three-dimensional shapes and Steiner's theorem [39]. The CoM for each component and its sub-components was estimated visually. The parameters mass (m), length (l), width (w), thickness (d), radius (r) and coordinates x, y and z will be given, specified with an subscript that indicates which component the parameter belongs to. Subscript c indicates that the inertia is given with respect to the (sub)components' own CoM. Since all inertia values of the original model were given with four significant digits, the same will be done for the new inertia. The resulting inertia matrices can be found in the last part of each respective section.

A.2.1 Conventional prosthesis

Socket

The socket (p) was divided in two parts: the top part was approached as a thin-walled cylinder (s), the bottom part was approached as a solid ball (b). All relevant parameters can be found in Table 5 and Fig. 17.

Table 5. Parameters for a conventional socket.
s: cylinder of the socket, b: ball of the socket

Parameter	Value	Unit
m_s	2.54	kg
l_s	0.2355	m
r_s	0.0738	m
$x_{s,c}$	0	m
$y_{s,c}$	0.0437	m
$z_{s,c}$	0	m
m_b	0.8000	kg
r_b	0.0042	m
$x_{b,c}$	0	m
$y_{b,c}$	-0.1441	m
$z_{b,c}$	0	m

$$I_{xx,sc} = \frac{1}{12} m_s (6r_s^2 + l_s^2) \tag{1}$$

$$I_{yy,sc} = m_s r_s^2 \tag{2}$$

$$I_{zz,sc} = \frac{1}{12} m_s (6r_s^2 + l_s^2) \tag{3}$$

$$I_{xx,bc} = \frac{2}{5} m_b r_b^2 \tag{4}$$

$$I_{yy,bc} = \frac{2}{5} m_b r_b^2 \tag{5}$$

$$I_{zz,bc} = \frac{2}{5} m_b r_b^2 \tag{6}$$

$$I_{xx,pc} = I_{xx,sc} + m_s (y_{s,c}^2 + z_{s,c}) + I_{xx,bc} + m_b (y_{b,c}^2 + z_{b,c}) \tag{7}$$

$$I_{yy,pc} = I_{xx,sc} + m_s (x_{s,c}^2 + z_{s,c}) + I_{xx,bc} + m_b (x_{b,c}^2 + z_{b,c}) \tag{8}$$

$$I_{zz,pc} = I_{xx,sc} + m_s (x_{s,c}^2 + y_{s,c}) + I_{xx,bc} + m_b (x_{b,c}^2 + y_{b,c}) \tag{9}$$

Lower leg
The lower leg of the prosthesis, which replaces the tibia and fibula, is modelled as a general shape and should not be taken too accurately. For the calculation of its inertia, a mean radius was calculated. The lower leg was approached as a solid cylinder. The radius was based on 0.6 times the radius of the upper part of the lower leg and 0.4 times the radius of the lower part of the lower leg. All relevant parameters can be found in Table 6 and Fig. 17.

Table 6. Parameters for a conventional lower leg. t: tibia

Parameter	Value	Unit
m_t	1.44	kg
l_t	0.3966	m
r_t	0.0162	m

$$I_{xx,tc} = \frac{1}{12} m_t (3r_t^2 + l_t^2) \tag{10}$$

$$I_{yy,tc} = \frac{1}{2} m_t r_t^2 \tag{11}$$

$$I_{zz,tc} = \frac{1}{12} m_t (3r_t^2 + l_t^2) \tag{12}$$

Foot
The complex form of the prosthetic foot was approximated as a solid cuboid (b) and solid cylinder (c). This however does not accurately describe the actual shape of the prosthesis. All relevant parameters can be found in Table 7 and Fig. 17.

Table 7. Parameters for a conventional foot. b: bottom block, c: upper cylinder, f: foot

Parameter	Value	Unit
m_b	0.35	kg
l_b	0.2286	m
d_b	0.0675	m
w_b	0.0424	m
$x_{b,c}$	0.019	m
$y_{b,c}$	-0.0194	m
$z_{b,c}$	0	m
m_u	0.24	kg
l_u	0.0281	m
r_u	0.0209	m
$x_{u,c}$	-0.0156	m
$y_{u,c}$	0.0193	m
$z_{u,c}$	0	m

$$I_{xx,bc} = \frac{1}{12} m_b (w_b^2 + d_b^2) \tag{13}$$

$$I_{yy,bc} = \frac{1}{12} m_b (l_b^2 + d_b^2) \tag{14}$$

$$I_{zz,bc} = \frac{1}{12} m_b (w_b^2 + l_b^2) \tag{15}$$

$$I_{xx,uc} = \frac{1}{12} m_u (3r_u^2 + l_u^2) \tag{16}$$

$$I_{yy,uc} = \frac{1}{2} m_u r_u^2 \tag{17}$$

$$I_{zz,uc} = \frac{1}{12} m_u (3r_u^2 + l_u^2) \tag{18}$$

$$I_{xx,fc} = I_{xx,bc} + m_s (y_{b,c}^2 + z_{b,c}) + I_{xx,uc} + m_u (y_{u,c}^2 + z_{u,c}) \tag{19}$$

$$I_{yy,fc} = I_{xx,bc} + m_s (x_{b,c}^2 + z_{b,c}) + I_{xx,uc} + m_u (x_{u,c}^2 + z_{u,c}) \tag{20}$$

$$I_{zz,fc} = I_{xx,bc} + m_s (x_{b,c}^2 + y_{b,c}) + I_{xx,uc} + m_u (x_{u,c}^2 + y_{u,c}) \tag{21}$$

Inertia matrices

$$\mathrm{I}_{\mathrm{socket}} = \begin{bmatrix} 0.0407 & 0 & 0 \\ 0 & 0.0144 & 0 \\ 0 & 0 & 0.0407 \end{bmatrix}, \qquad \mathrm{I}_{\mathrm{tibia}} = \begin{bmatrix} 0.0190 & 0 & 0 \\ 0 & 0.0002 & 0 \\ 0 & 0 & 0.0190 \end{bmatrix}, \qquad \mathrm{I}_{\mathrm{foot}} = \begin{bmatrix} 0.0004 & 0 & 0 \\ 0 & 0.0019 & 0 \\ 0 & 0 & 0.0020 \end{bmatrix}$$

A.2.2 WalkMECH prosthesis

Socket
Since the knee joint of the Unal prosthesis is equal to that of the conventional prosthesis, the same component, and therefore the same inertia matrix can be used.

Lower leg
Because the ankle joint for the Unal prosthesis is slightly lower than for the conventional prosthesis, the length of the prosthesis was calculated accordingly and set to 0.4374 m (see Fig. 18). Equations 10 to 12 were used with the new length. All other parameters were kept equal.

Foot
The foot that was used for the final model was slightly different from the foot described here. Nonetheless, the same inertia values were used. The foot used by Unal is considerably different from a conventional foot. For calculating the inertia, it was approximated by three solid cuboids of two different sizes and a solid cylinder. All relevant parameters can be found in Table 8 and Fig. 18.

Table 8. Parameters for the foot for the Unal prosthesis. p1: side plate (2x), p2: bottom plate, r: rod that makes up joint, f: foot

Parameter	Value	Unit
m_{p1}	0.167	kg
l_{p1}	0.24	m
d_{p1}	0.0085	m
w_{p1}	0.0676	m
$x_{p1,c}$	0.0194	m
$y_{p1,c}$	0.0061	m
$z_{p1,c}$	0.0414	m
m_{p2}	0.167	kg
l_{p2}	0.24	m
d_{p2}	0.0052	m
w_{p2}	0.0809	m
$x_{p1,c}$	-0.0194	m
$y_{p2,c}$	0.0248	m
$z_{p2,c}$	0	m
m_r	0.15	kg
l_r	0.0686	m
r_r	-0.0140	m
$x_{r,c}$	-0.0344	m
$y_{r,c}$	0	m
$z_{r,c}$	0	m

$$I_{xx,p1c} = \frac{1}{12} m_{p1}(w_{p1}^2 + d_{p1}^2) \tag{22}$$

$$I_{yy,p1c} = \frac{1}{12} m_{p1}(l_{p1}^2 + d_{p1}^2) \tag{23}$$

$$I_{zz,p1c} = \frac{1}{12} m_{p1}(w_{p1}^2 + l_{p1}^2) \tag{24}$$

$$I_{xx,p2c} = \frac{1}{12} m_{p2}(w_{p2}^2 + d_{p2}^2) \tag{25}$$

$$I_{yy,p2c} = \frac{1}{12} m_{p2}(l_{p2}^2 + d_{p2}^2) \tag{26}$$

$$I_{zz,p2c} = \frac{1}{12} m_{p2}(w_{p2}^2 + l_{p2}^2) \tag{27}$$

$$I_{xx,rc} = \frac{1}{12} m_r(3r_r^2 + l_r^2) \tag{28}$$

$$I_{yy,rc} = \frac{1}{12} m_r(3r_r^2 + l_r^2) \tag{29}$$

$$I_{zz,rc} = \frac{1}{2} m_r r_r^2 \tag{30}$$

$$\begin{aligned} I_{xx,fc} = {} & 2(I_{xx,p1c} + m_s(y_{p1,c}^2 + z_{p1,c})) + I_{xx,p2c} \\ & + m_s(y_{p2,c}^2 + z_{p2,c}) + I_{xx,rc} + m_r(y_{r,c}^2 + z_{r,c}) \end{aligned} \tag{31}$$

$$\begin{aligned} I_{yy,fc} = {} & 2(I_{xx,p1c} + m_s(x_{p1,c}^2 + z_{p1,c})) + I_{xx,p2c} \\ & + m_s(x_{p2,c}^2 + z_{p2,c}) + I_{xx,rc} + m_r(x_{r,c}^2 + z_{r,c}) \end{aligned} \tag{32}$$

$$\begin{aligned} I_{zz,fc} = {} & 2(I_{xx,p1c} + m_s(x_{p1,c}^2 + y_{p1,c})) + I_{xx,p2c} \\ & + m_s(x_{p2,c}^2 + y_{p2,c}) + I_{xx,rc} + m_r(x_{r,c}^2 + y_{r,c}) \end{aligned} \tag{33}$$

Sliders

The sliders to which the distal end of the spring attach were approached as solid cubes. All relevant parameters can be found in Table 9 and Fig. 18.

Table 9. Parameters for the slider for the foot by Unal. s: slider

Parameter	Value	Unit
m_s	0.1	kg
l_s	0.0335	m
d_s	0.0103	m
w_s	0.0163	m

$$I_{xx,sc} = \frac{1}{12} m_s(w_s^2 + d_s^2) \tag{34}$$

$$I_{yy,sc} = \frac{1}{12} m_s(l_s^2 + d_s^2) \tag{35}$$

$$I_{zz,sc} = \frac{1}{12} m_s(w_s^2 + l_s^2) \tag{36}$$

Inertia matrices

$$\mathrm{I}_{\mathrm{tibia}} = \begin{bmatrix} 0.0231 & 0 & 0 \\ 0 & 0.0002 & 0 \\ 0 & 0 & 0.0231 \end{bmatrix}, \qquad \mathrm{I}_{\mathrm{foot}} = \begin{bmatrix} 0.0010 & 0 & 0 \\ 0 & 0.0034 & 0 \\ 0 & 0 & 0.0031 \end{bmatrix},$$

$$\mathrm{I}_{\mathrm{slider}} = \begin{bmatrix} 0.0000 & 0 & 0 \\ 0 & 0.0000 & 0 \\ 0 & 0 & 0.0000 \end{bmatrix}$$

A.3 Modelling details

To model the blocking mechanism of the walkMECH, an expression based point to point force was implemented. The expression was an exponential equation that describes a strong force at low distance and a very low force at high distance. The equation used is $F_{mag} = 0.0003/d^2$, in which d is the distance between the slider and the front of the sliding slot.

The curved slider slot of the walkMECH was modelled as a custom joint. The movement along the x-axis was specified by a linear function with coefficients 1 and 0. The movement along the y-axis was specified by a stepfunction with a transition between -0.04 and -0.046m and a change in value from 0 to -0.006m.

Both springs in the walkMECH were modelled as expression based point to point forces. The foot spring prevents plantarflexion. The equation formulated for the foot spring is as follows:
$F_{Ci,j} = \frac{k_{Ci,j}}{2}(l_{Ci} - l_{rest,i} - l_{slack,Ci,j}) + \frac{k_{Ci,j}}{2}|l_{Ci} - l_{rest,i} - l_{slack,Ci,j}|$
In this equation, i is replaced by the number of the spring, with 1 for the biarticular spring (C1) and 2 for the foot spring (C2). For the biarticular spring, j is replaced by either 1, referring to the outer spring, or 2, referring to the inner spring. For the foot spring, j is left out because there is only one spring. k is the stiffness of the spring. l_{Ci} is the current length of the spring, $l_{rest,i}$ is the distance between the attachment points at which the slacklength of the spring occurs and l_{slack} is the slacklength of the spring. To calculate the total force of the biarticular spring, the forces of the inner and outer spring should be added as $F_{C1} = F_{C1,1} + FC1,2$. The force-length relationships of both springs can be found in Fig. 5.

A.4 SCONE files

In the main script, simulation parameters are defined, such as the minimum progress of the optimisation steps, the initial parameters (optional) and the maximum duration of the objective. The minimum progress and maximum duration were set to $1e^{-4}$ and 10s respectively. The initial parameters and a standard deviation offset were defined in a later stage of the process. The initial state file was set, as well as initial state offsets [20]. The offsets of all states except those ending with _tx, _ty and _u were set to $0 \sim 0.01 < -0.5, 0.5 >$. The properties of the model that need to be optimised must be included to this file as well. For the prosthetic leg, the stiffness and damping of the prosthetic joints were optimised. The mean and extreme values were estimated based on preliminary simulations. Lastly, two files need to be called on: the controller and the measure for the gait pattern.

The controller script includes conditional controllers for reflexes. First, the stance load threshold is defined to be able to discriminate between the gait phases. Furthermore, because the model is asymmetric, "symmetric = 0" is included. After these lines, conditional controllers are defined for different muscles or muscle groups and for different states. After the statement of the states and the leg the controller applies to, the type of controller is defined. Dependent on the type of controller, the target muscle, source, delay, dof, KL, KF, KP, KV, L0, pos_max, P0 and/or C0 are included. The source can be either another muscle or a degree of freedom. The delay is given in seconds and represents the neuromuscular delay, which is zero if not defined. The dof is the degree of freedom

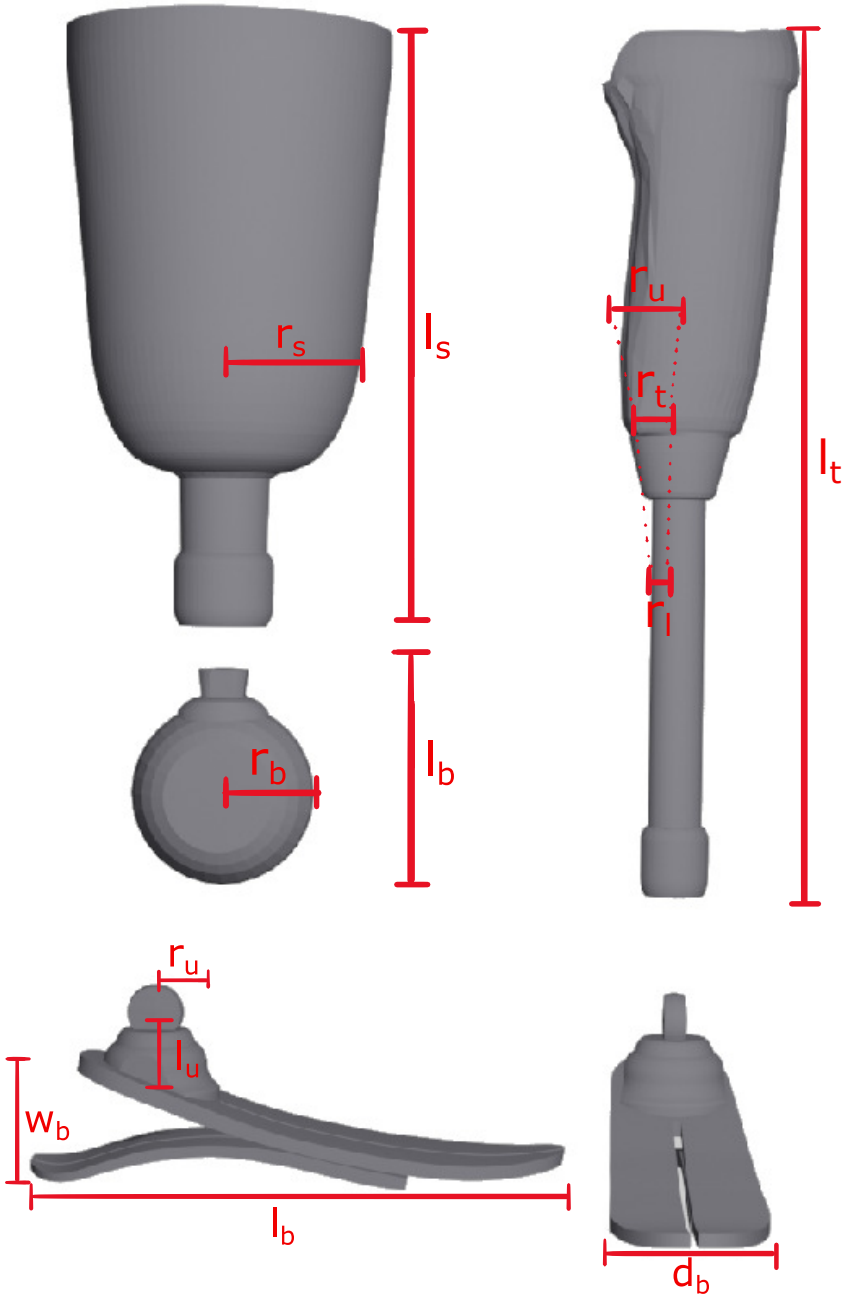

Fig 17. Conventional prosthesis geometry. Geometry of conventional prosthetic parts with measurement indications. Top left: side view of socket. Middle left: side view of upper part of knee joint. Top right: side view of lower leg. Bottom left: side view of foot. Bottom right: front view of foot.

involved, such as knee_angle. For the following parameters, a standard deviation, minimum and maximum value are defined ($\sim$ std $<$ min, max $>$). The KL, KF, KP and KV are the length, force, position and velocity feedback gain respectively. Each feedback gain is based on its normalised parameter and is zero per default. L0 is the length feedback offset, which is 1 if not defined. pos_max is the maximum DOF position in which the reflex is active. The maximum position is given in radians or meters and $-$1e12 per default. L0 is the length feedback offset, which is set to 0 when not

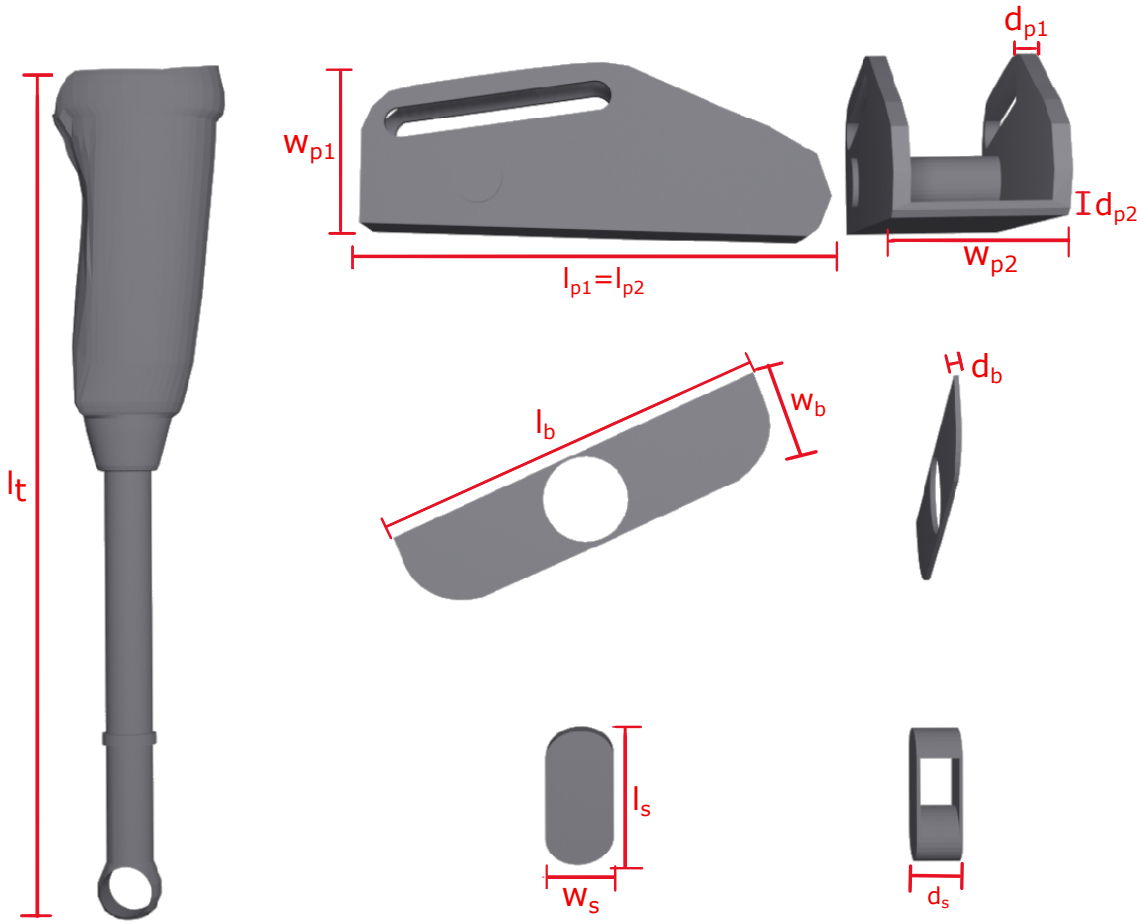

Fig 18. WalkMECH prosthesis geometry. Geometry of prosthetic parts for the walkMECH prosthesis with measurement indications [14]. Left: Side view of lower leg. Top right: Side and front view of foot. Middle right: side and front view of blocker plate. Bottom right: Side and front view of slider. Note: the proportions of the prosthetic parts with respect to each other are not realistic.

defined. P0 is the target position for the sensor DOF in radians or meters and C0 is the constant actuation added to the reflex. Both parameters are zero per default. A full list of parameters that can be defined in the controllers can be found in the SCONE documentation [34].

The muscle parameters were mostly copied from the provided file. However, the amputated muscles were removed.

The measures script includes all measures that need to be minimised. In this case, a gait measure, effort measure, composite measure and reaction force measure are included. The script was copied fully from that for a healthy gait optimisation. The gait measure was set to weight the most by far (100), followed by the reaction force measure (10), the effort measure (0.1), DOF measure for the ankle angle (0.1) and for the knee angle (0.01). The minimum and maximum velocity in the gait measure were set to 0.8m/s and 0.95m/s respectively. This speed was chosen based on preliminary simulations and experimental data [7]. For the effort measure, measure type Uchida2016 was used.

A simulation that was terminated after minimum progress was reached was first judged based on its fitness score. The lower the fitness score, the better the result meets the cost functions. In order to eliminate results that stopped at a local minimum, all simulations were run multiple times. The fitness score was desired to be two or lower. Whenever a result reached this fitness, it was examined visually. Firstly, the generated gait pattern should not appear too different from either a healthy or

prosthetic gait pattern. Secondly, it was made sure that all limitations imposed by limit forces were indeed enforced. For instance, if a limit was exceeded significantly, the result was not used. Lastly, the effects of the actuator, if present, was assessed. The direction and timing of the applied force were examined and if those were not realistic or as intended, the result was omitted and the model was adapted accordingly.

A.5 Joint loads

The joint loads resulting from the predictive simulations were excluded from the results because we could not properly compare them to experimental data and the results were inconclusive. The only conclusion that can be drawn from the results is that for none of the models and none of its joints, the joint loads became high enough to be harmful for the healthy of the person. A high joint load would increase the risk for e.g. osteoarthritis [40].

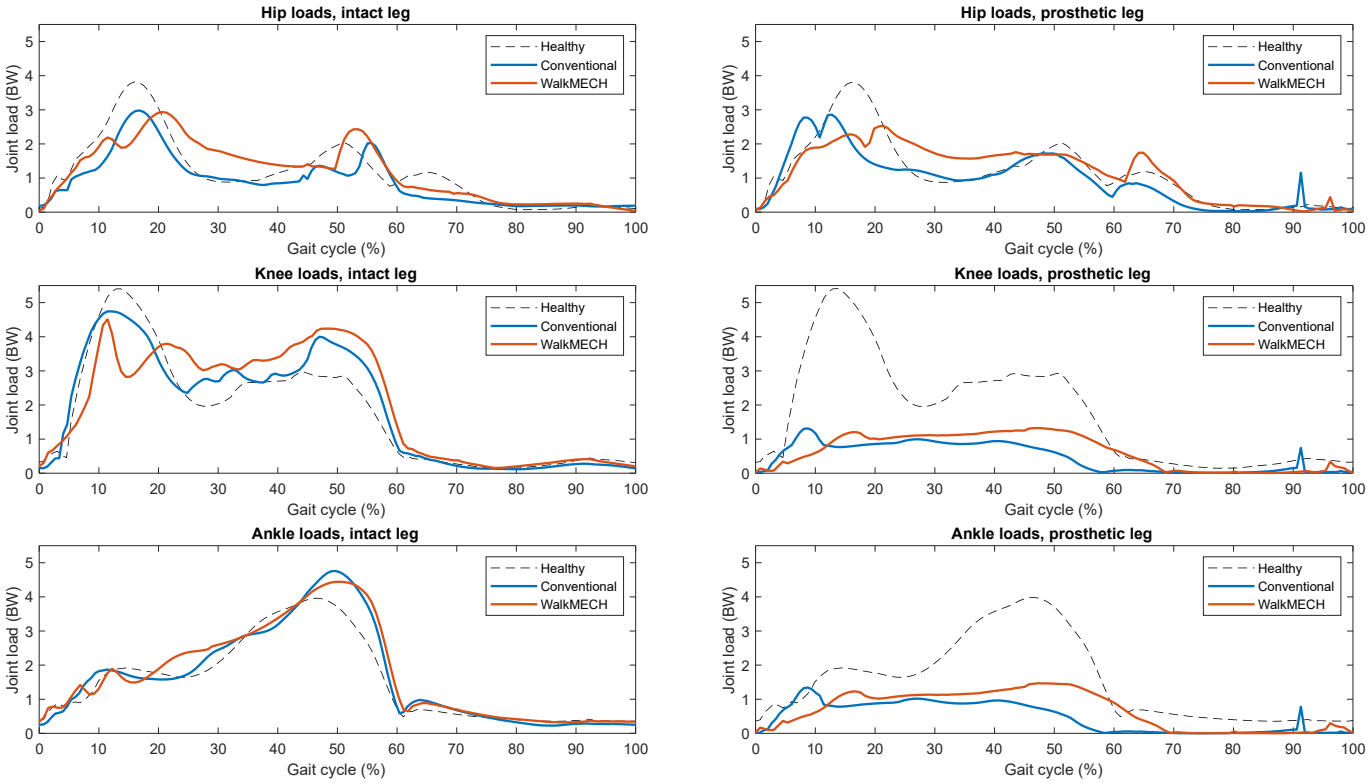

Fig 19. Joint loads. Joint loads for the three main models: HM, CM and WM.

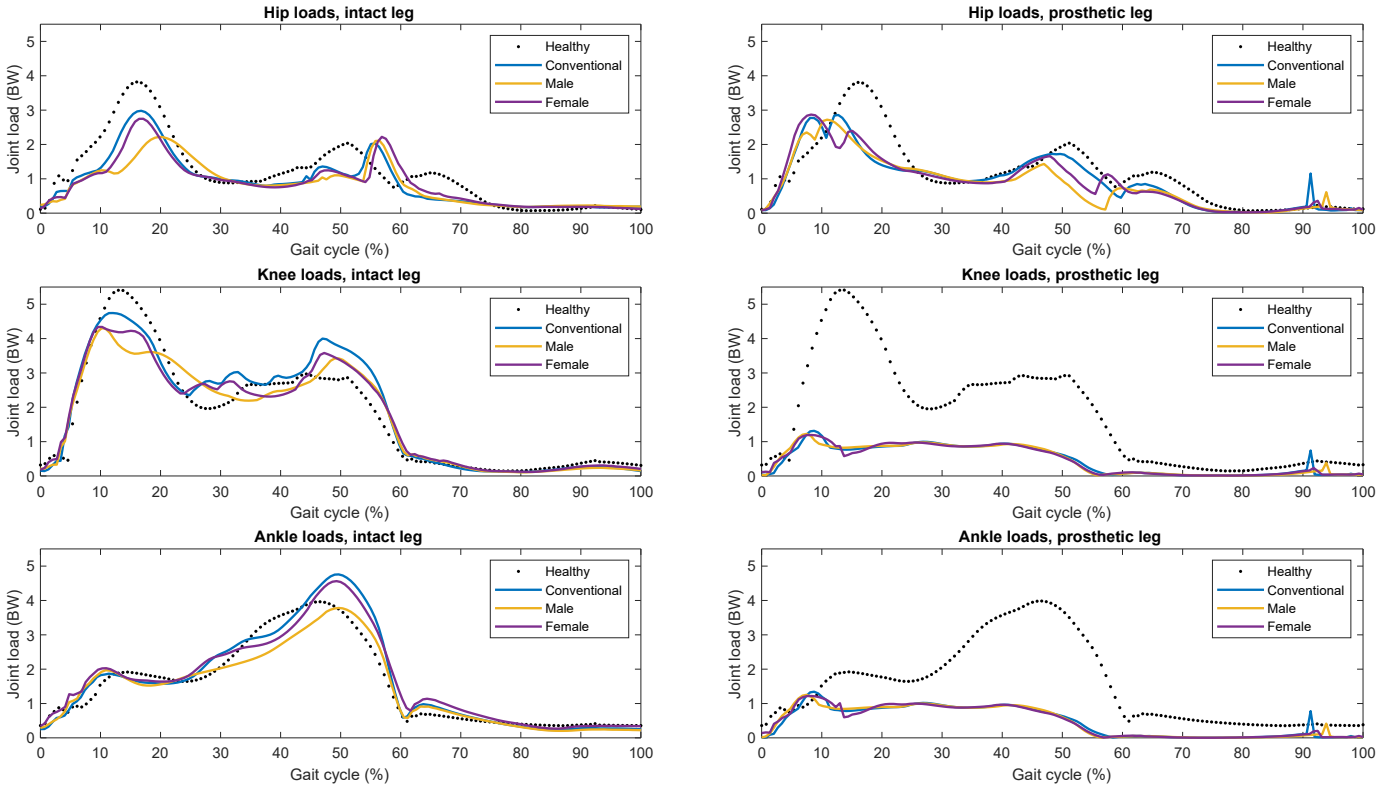

Fig 20. Conventional prosthesis joint loads. Joint loads for the conventional prosthesis model and its scaled models: CM, CMm and CMf.

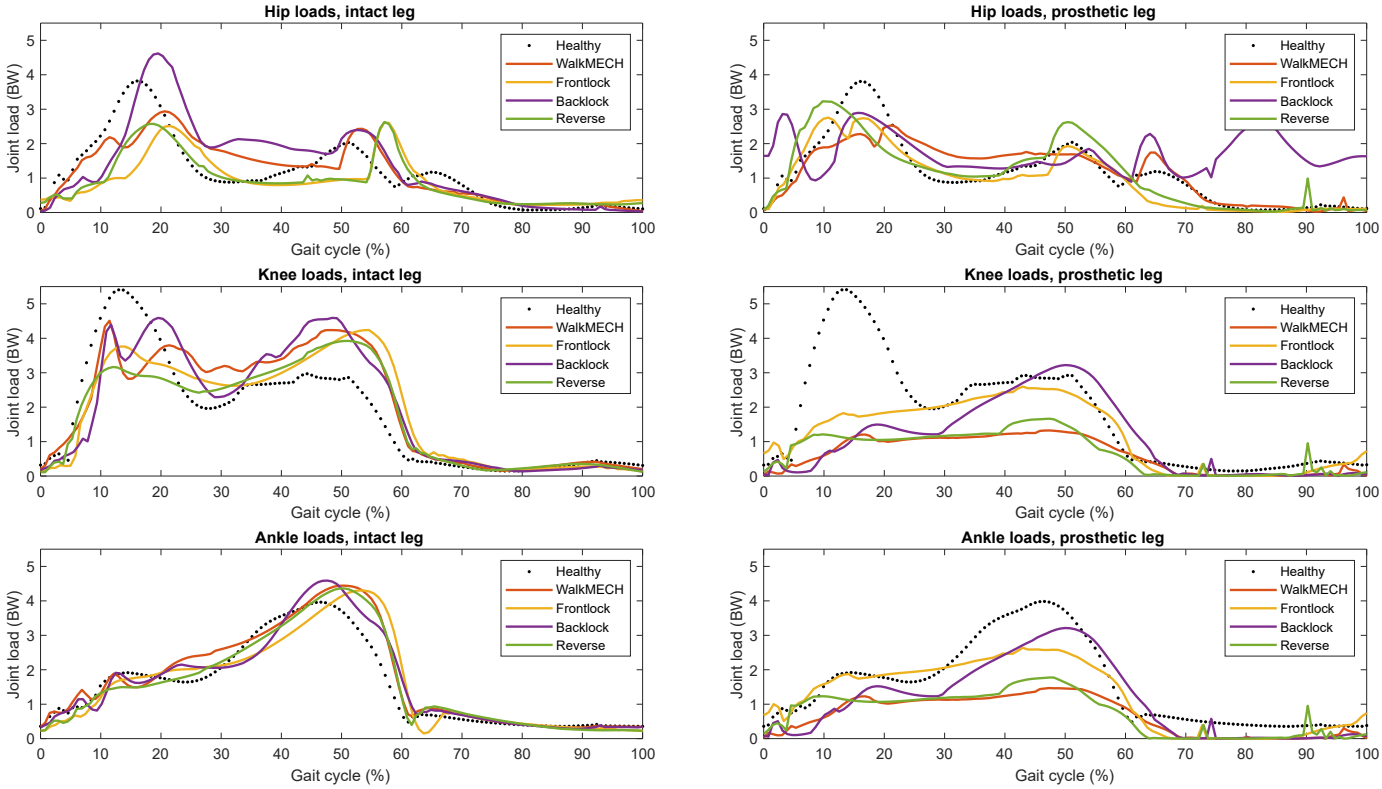

Fig 21. WalkMECH prosthesis joint loads. Joint loads for the walkMECH prosthesis model and its variations: WM, WMf, WMb and WMr.